Contents lists available at ScienceDirect

Environment International

journal homepage: www.elsevier.com/locate/envint

Full length article

European aerosol phenomenology − 8: Harmonised source apportionment of organic aerosol using 22 Year-long ACSM/AMS datasets

Gang Chen [a], Francesco Canonaco [a,b], Anna Tobler [a,b], Wenche Aas [c], Andres Alastuey [d], James Allan [e,f], Samira Atabakhsh [g], Minna Aurela [h], Urs Baltensperger [a], Aikaterini Bougiatioti [i], Joel F. De Brito [j], Darius Ceburnis [k], Benjamin Chazeau [a,l,m], Hasna Chebaicheb [j,n], Kaspar R. Daellenbach [a], Mikael Ehn [o], Imad El Haddad [a], Konstantinos Eleftheriadis [p], Olivier Favez [n], Harald Flentje [q], Anna Font [r,1], Kirsten Fossum [k], Evelyn Freney [s], Maria Gini [p], David C Green [r,t], Liine Heikkinen [o,2], Hartmut Herrmann [g], Athina-Cerise Kalogridis [p], Hannes Keernik [u,v], Radek Lhotka [w,x], Chunshui Lin [k], Chris Lunder [c], Marek Maasikmets [u], Manousos I. Manousakas [a], Nicolas Marchand [l], Cristina Marin [y,z], Luminita Marmureanu [y], Nikolaos Mihalopoulos [i], Griša Močnik [aa,ab], Jaroslaw Nęcki [ac], Colin O'Dowd [k], Jurgita Ovadnevaite [k], Thomas Peter [ad], Jean-Eudes Petit [ae], Michael Pikridas [af], Stephen Matthew Platt [c], Petra Pokorná [w], Laurent Poulain [g], Max Priestman [r], Véronique Riffault [j], Matteo Rinaldi [ag], Kazimierz Różański [ac], Jaroslav Schwarz [w], Jean Sciare [af], Leïla Simon [n,ae], Alicja Skiba [ae], Jay G. Slowik [a], Yulia Sosedova [b], Iasonas Stavroulas [i,af], Katarzyna Styszko [ah], Erik Teinemaa [u], Hilkka Timonen [h], Anja Tremper [r,t], Jeni Vasilescu [y], Marta Via [d,ai], Petr Vodička [w], Alfred Wiedensohler [g], Olga Zografou [p], María Cruz Minguillón [d,*], André S.H. Prévôt [a,*]

[a] Laboratory of Atmospheric Chemistry, Paul Scherrer Institute, 5232 Villigen, Switzerland
[b] Datalystica Ltd., Park innoAARE, 5234 Villigen, Switzerland
[c] NILU - Norwegian Institute for Air Research, 2007 Kjeller, Norway
[d] Institute of Environmental Assessment and Water Research (IDAEA), Spanish Council for Scientific Research (CSIC), Barcelona, 08034, Spain
[e] Department of Earth and Environmental Sciences, University of Manchester, Manchester, UK
[f] National Centre for Atmospheric Science, University of Manchester, Manchester, UK
[g] Department of Chemistry of the Atmosphere Leibniz Institute for Tropospheric Research, Permoser Straße 15, 04318 Leipzig, Germany
[h] Atmospheric Composition Research, Finnish Meteorological Institute, P.O. Box 503, 00101 Helsinki, Finland
[i] Institute for Environmental Research and Sustainable Development, National Observatory of Athens, Palaia Penteli, 15236 Athens, Greece
[j] IMT Nord Europe, Institut Mines-Télécom, Univ. Lille, Centre for Energy and Environment, 59000 Lille, France
[k] School of Physics, Ryan Institute's Centre for Climate and Air Pollution Studies, National University of Ireland Galway, University Road, Galway H91 CF50, Ireland
[l] Aix Marseille Univ., CNRS, LCE, Marseille, France
[m] AtmoSud, Regional Network for Air Quality Monitoring of Provence-Alpes-Côte-d'Azur, Marseille, France
[n] Institut National de l'Environnement Industriel et des Risques, Parc Technologique ALATA, 60550, Verneuil en Halatte, France
[o] Institute for Atmospheric and Earth System Research (INAR)/Physics, University of Helsinki, Helsinki, Finland
[p] Environmental Radioactivity Laboratory, Institute of Nuclear & Radiological Sciences & Technology, Energy & Safety, N.C.S.R. "Demokritos", 15310 Athens, Greece
[q] Deutscher Wetterdienst, Meteorologisches Observatorium Hohenpeißenberg, 82383 Hohenpeißenberg, Germany
[r] MRC Centre for Environment and Health, Environmental Research Group, Imperial College London, 86 Wood Lane, London W12 0BZ, UK
[s] Laboratoire de Météorologie Physique, UMR6016, Université Clermont Auvergne-CNRS, Aubière, France
[t] HPRU in Environmental Exposures and Health, Imperial College London, UK
[u] Air Quality and Climate Department, Estonian Environmental Research Centre (EERC), Marja 4D, Tallinn, Estonia
[v] Department of Software Science, Tallinn University of Technology, 19086 Tallinn, Estonia
[w] Institute of Chemical Process Fundamentals of the CAS, Rozvojová 135/1, 16502 Prague, Czech Republic
[x] Institute for Environmental Studies, Faculty of Science, Charles University, Benátská 2, 12801 Prague, Czech Republic
[y] National Institute of Research and Development for Optoelectronics INOE 2000, 77125 Magurele, Romania
[z] Department of Physics, Politehnica University of Bucharest, Bucharest,Romania

* Corresponding authors.
  E-mail addresses: mariacruz.minguillon@idaea.csic.es (M. Cruz Minguillón), andre.prevot@psi.ch (A.S.H. Prévôt).

aa *Condensed Matter Physics Department, J. Stefan Institute, Ljubljana, Slovenia*
ab *Center for Atmospheric Research, University of Nova Gorica, Ajdovščina, Slovenia*
ac *AGH University of Science and Technology, Faculty of Physics and Applied Computer Science, Department of Applied Nuclear Physics, Kraków, Poland*
ad *Institute for Atmospheric and Climate Sciences, ETH Zürich, Zürich, 8092, Switzerland*
ae *Laboratoire des Sciences du Climat et de l'Environnement, UMR 8212, CEA/Orme des Merisiers, 91191 Gif-sur-Yvette, France*
af *Climate & Atmosphere Research Centre (CARE-C), The Cyprus Institute, Nicosia, 2121, Cyprus*
ag *Institute of Atmospheric Sciences and Climate (ISAC), National Research Council (CNR), 40129 Bologna, Italy*
ah *AGH University of Science and Technology, Faculty of Energy and Fuels, Department of Coal Chemistry and Environmental Sciences, Kraków, Poland*
ai *Department of Applied Physics, University of Barcelona, Barcelona 08028, Spain*

A R T I C L E I N F O	A B S T R A C T
Handling Editor: Adrian Covaci	Organic aerosol (OA) is a key component of total submicron particulate matter (PM$_1$), and comprehensive knowledge of OA sources across Europe is crucial to mitigate PM$_1$ levels. Europe has a well-established air quality research infrastructure from which yearlong datasets using 21 aerosol chemical speciation monitors (ACSMs) and 1 aerosol mass spectrometer (AMS) were gathered during 2013–2019. It includes 9 non-urban and 13 urban sites. This study developed a state-of-the-art source apportionment protocol to analyse long-term OA mass spectrum data by applying the most advanced source apportionment strategies (i.e., rolling PMF, ME-2, and bootstrap). This harmonised protocol was followed strictly for all 22 datasets, making the source apportionment results more comparable. In addition, it enables quantification of the most common OA components such as hydrocarbon-like OA (HOA), biomass burning OA (BBOA), cooking-like OA (COA), more oxidised-oxygenated OA (MO-OOA), and less oxidised-oxygenated OA (LO-OOA). Other components such as coal combustion OA (CCOA), solid fuel OA (SFOA: mainly mixture of coal and peat combustion), cigarette smoke OA (CSOA), sea salt (mostly inorganic but part of the OA mass spectrum), coffee OA, and ship industry OA could also be separated at a few specific sites. Oxygenated OA (OOA) components make up most of the submicron OA mass (average = 71.1%, range from 43.7 to 100%). Solid fuel combustion-related OA components (i.e., BBOA, CCOA, and SFOA) are still considerable with in total 16.0% yearly contribution to the OA, yet mainly during winter months (21.4%). Overall, this comprehensive protocol works effectively across all sites governed by different sources and generates robust and consistent source apportionment results. Our work presents a comprehensive overview of OA sources in Europe with a unique combination of high time resolution (30–240 min) and long-term data coverage (9–36 months), providing essential information to improve/validate air quality, health impact, and climate models.

1. Introduction

Atmospheric aerosols are liquid or solid particles suspended in the atmosphere (Hinds, 1999), which cause serious adverse health effects, reduce visibility, and interact with ecosystems and climate (IPCC, 2021). Despite all efforts, Europe is still suffering from poor air quality. Specifically, the European Environment Agency (EEA) (2021) reported that 2% of the reporting countries exceeded the annual PM$_{2.5}$ (atmospheric particulate matter (PM) with an aerodynamic diameter of 2.5 μm or less) limit value of EU legislation (25 μg/m³) in 2019. Following the even stricter 2021 WHO PM$_{2.5}$ guidelines (5 μg/m³), all reporting countries, except Estonia, were over the limit that year (European Environment Agency (EEA), 2021; World Health Organization, 2021). Therefore, it is more important than ever to mitigate the air pollution levels. Moreover, premature deaths attributed to long-term exposure to PM$_{2.5}$ in 27 EU member states reached 307,000 in 2019 (European Environment Agency (EEA), 2021). As one of the most significant aerosol components, organic aerosol (OA) gained extensive interest since it represents 20 to 90% of the mass of the total submicron aerosol (Crippa et al., 2014; Jimenez et al., 2009; Zhang et al., 2011, 2007). Importantly, a simple reduction of PM$_{2.5}$ or even OA might not be an effective strategy to mitigate the health impacts of aerosol because OA components from different sources have different toxicities (Daellenbach et al., 2020). In addition, various sources/compositions of OA can also have significant differences in climate forcing (Yang et al., 2018). Therefore, a comprehensive knowledge of the OA sources could provide more information for regional, global climate, or air quality models for emission inventories, parameterization, or validation.

Typically, OA sources are identified using the receptor model positive matrix factorisation (PMF) on data from an Aerodyne aerosol mass spectrometer (AMS; (Jayne et al., 2000)). Many studies have reported a broad spatial overview of OA sources, providing the chemical composition of the bulk non-refractory PM$_1$ and, more recently, also PM$_{2.5}$ (Elser et al., 2016; Xu et al., 2017). Zhang et al. (2007) first reviewed the use of factor analysis to investigate OA sources in urban and rural/remote sites in the Northern Hemisphere. Jimenez et al. (2009) provided an overview of PM$_1$ chemical composition and OA sources worldwide (including eight European sites), while Ng et al. (2010) provided a big picture of OA sources over the Northern Hemisphere in various environments (including 43 AMS datasets). PM$_1$ chemical composition and OA sources in Central Europe, including Switzerland, Germany, Austria, France, and Liechtenstein, have been described more specifically in Lanz et al. (2010). Finally, an overview of the OA sources across Europe using 25 AMS datasets, combined with guidelines for source apportionment (SA) applications to AMS data, resulted from the work of (Crippa et al., 2014). However, the AMS requires labour-intensive maintenance, making it extremely difficult to run continuously over a long period. Most of the AMS datasets in previous studies only covered time periods up to a few months, and the seasonal variations of OA sources in Europe remain mostly unknown without consistent long-term SA studies. Therefore, a network of on-line chemical composition measurements has been built up within the well-established European Aerosol, Clouds and Trace gases Research InfraStructure (ACTRIS, http://actris.eu), consisting of 1 AMS and 21 Aerodyne Aerosol Chemical Speciation Monitors (ACSM, (Fröhlich et al., 2013; Ng et al., 2011b)), the latter being a simpler and more robust version of the AMS. With these data, it is possible to address a critical knowledge gap in the literature, i.e., the seasonal, diurnal, and spatial variabilities of OA sources across Europe.

An important limitation of the conventional PMF applications for long-term datasets is that OA sources are assumed to be static over the entire sampling period, although the source profiles of OA have substantial seasonal variations (Canonaco et al., 2015; Crippa et al., 2014;

---

[1] Now at: IMT Nord Europe, Institut Mines-Télécom, Univ. Lille, Centre for Energy and Environment, 59000 Lille, France.
[2] Now at: Department of Environmental Science & Bolin Centre for Climate Research, Stockholm University, Stockholm, Sweden.

Zhang et al., 2019). This study applies a novel SA technique, rolling PMF (Canonaco et al., 2021; Parworth et al., 2015), to account for the temporal variabilities of the factor profiles. Instead of running PMF for the whole dataset, this work applies a smaller time window (e.g., varying from 7 to 28 days), moving with daily steps over the entire dataset (typically around one year). This allows the model to gradually adapt the factor profiles across different observational periods. In addition, the rolling technique has been equipped with random input resampling and random variation of the constraints allowing for a quantitative estimate of the statistical and rotational uncertainties of the PMF solutions (Canonaco et al., 2021; Chen et al., 2021). Meanwhile, rolling PMF can facilitate the analysis while handling the long-term ACSM/AMS datasets by saving computational time compared to conventional seasonal bootstrap PMF.

The comparison of SA results from different sites is challenging, as they are not always equivalent due to the subjective decisions made by the analysts during the different PMF analysis steps, especially regarding the optimal number of factors, their identification, and validation. For that reason, a standardised protocol (Section 2.3) has been developed to ensure comparability between results obtained from different sites/instruments. According to this protocol, rolling PMF is performed following the latest and most advanced statistical features present within the Source Finder Professional (SoFi Pro) package (Datalystica Ltd., Villigen, Switzerland, (Canonaco et al., 2021, 2013)) integrated into the Igor Pro software (WaveMetrics Inc., Lake Oswego, OR, USA). Although subjective judgements cannot be avoided entirely, the developed protocol aims to minimise the number of decisions to be made by the user.

This highly time-resolved information of OA sources in Europe could substantially improve the development, validation, and prediction of regional/global air quality/climate models by providing extra independent information. These results could also be helpful to health-related studies when trying to accurately predict the toxicity of atmospheric aerosol since OA has significantly different health impacts depending on its origin (Daellenbach et al., 2020). Multiple years of data are finally needed to assess the impact of particulate matter sources on morbidity and mortality due to chronic exposure (Liu et al., 2019; Yang et al., 2019). Eventually, this work will provide valuable information for policymakers to take the most effective mitigation measures for aerosol-related environmental problems. Overall, this study presents a comprehensive overview of OA sources across Europe by following a thoroughly-designed and harmonised protocol (Section 2.3).

Specifically, the seasonal/spatial variability of OA sources regarding time series and source profiles are unfolded in the following sections.

2. Measurements and instrumentation

This study is the main outcome of the Chemical On-Line cOmpoSition and Source Apportionment of fine aerosoL (COLOSSAL) project (https://www.costcolossal.eu/), based on measurements performed within ACTRIS. In total, 22 year-long datasets were used here from 14 different countries via ACSM/AMS since 2013 (Fig. 1). This study includes data from 18 Q-ACSM (quadrupole ACSM, (Ng et al., 2011b)), 3 ToF-ACSM (Time-of-Flight ACSM (Fröhlich et al., 2013)), and 1 C-ToF-AMS (compact time-of-flight AMS (Drewnick et al., 2005)).

Overall, the ACSM and AMS considered here apply similar techniques. Briefly, the air is passing through a critical orifice into an aerodynamic lens, where atmospheric aerosol is focused and accelerated (the smaller the aerodynamic size, the higher the velocity) into a vacuum chamber (10^{-5} Torr) and impacts on the surface of a standard vaporiser heated at 600 °C. The resulting vapours are then ionised by electron ionisation (70 eV), and these ions are further extracted into the mass analyzer. Compared to the AMS, the ACSM is more robust, affordable, and easier to operate, making it suitable for long-term monitoring purposes. However, it cannot measure the size-resolved chemical composition and its time and mass resolutions are poorer compared to the AMS. Most of the ACSMs deployed here participated in an inter-comparison activity conducted by the Aerosol Chemical Monitor Calibration Centre (ACMCC) at SIRTA (https://sirta.ipsl.fr/) and reported consistent results as long as proper calibrations were conducted (Crenn et al., 2015; Freney et al., 2019). One of the objectives of the COLOSSAL project is to deliver a harmonised standard operating procedure (SOP) for ACSMs (COLOSSAL, 2021), and most of the 22 datasets were collected by following this SOP. However, the recommended relative ionisation efficiency (RIE) calibration procedures have varied over the long-time span of these datasets (2013–2019). For instance, some of the datasets conducted RIE calibration only on specific m/z values (jump scan) as recommended earlier, instead of scanning the entire mass range (m/z 10 to 150) of the mass spectrometer (Freney et al., 2019). Considering the nitrate interference on the CO_2^+ signal at m/z 44 (so-called Pieber effect) is time-dependent (Freney et al., 2019; Fröhlich et al., 2015; Pieber et al., 2016) and m/z 44 is not measured in jump scan RIE calibrations, it is thus impossible to do a post-correction consistently. Therefore, none of the datasets was corrected for the Pieber
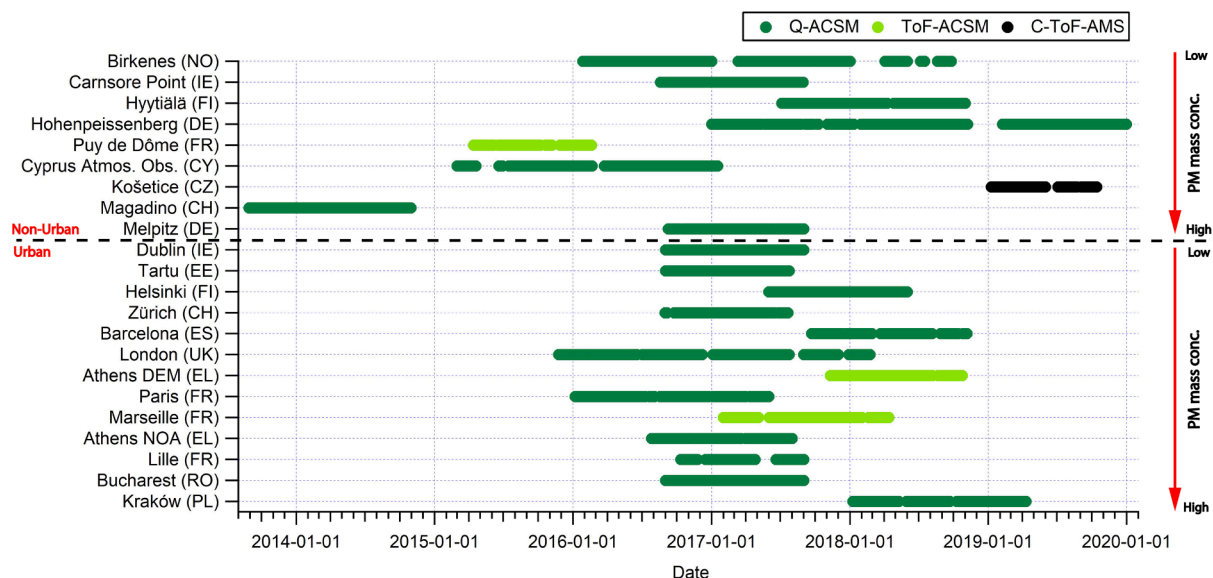

Fig. 1. ACSM/AMS measurement periods considered in this study.

effect. However, it is assumed that such artefact would not represent more than 25% (as maximum, e.g., during severe ammonium nitrate pollution episodes) of total OA readings by AMS/ACSM used for the present study.

Complementary to ACSM/AMS measurements, equivalent black carbon (eBC) was also monitored at all sites using filter-based absorption photometers. It was typically measured using Multi Angle Absorption Photometer (MAAP) (Thermo) or Aethalometer Model AE33 (Magee Scientific) devices and predominantly with default settings as proposed by the manufacturer (i.e., with no extra data correction procedures). In the case of multi-wavelength instruments (e.g., AE33 or former AE31 devices), eBC concentrations were reported from measurements at 880 nm, and solid/liquid fuel-burning eBC subfractions (noted eBC$_{wb}$ and eBC$_{ff}$, for wood burning, and fossil fuel, respectively, hereafter) were distinguished from each other based on the application of the so-called Aethalometer model (Sandradewi et al., 2008; Zotter et al., 2017).

The 22 sampling sites are classified based on their geographic locations as urban (13 sites, including four flagged as suburban: Athens DEM, Lille, Paris, and Bucharest) or non-urban (9 sites, Table S1). The chemical composition of some of these 22 datasets have already been reported (Barreira et al., 2021; Bressi et al., 2021). This study focuses on the overview of OA source apportionment results and includes new sites in our analysis. More details about source apportionment results at some of these sites can be found in the following published papers: (Barreira et al., 2021; Canonaco et al., 2021; Chazeau et al., 2022, 2021; Chen et al., 2021; Farah et al., 2021; Heikkinen et al., 2021; Lin et al., 2019; Minguillón et al., 2015; Petit et al., 2021; Poulain et al., 2020; Stavroulas et al., 2019; Tobler et al., 2021; Via et al., 2021; Yttri et al., 2021; Zhang et al., 2019).

2.1. Positive matrix factorisation (PMF) and multilinear engine (ME-2)

PMF has been customarily performed to conduct source apportionment of ambient aerosol data (e.g., ACSM/AMS data) in many previous studies (Lanz et al., 2007; Ulbrich et al., 2009; Zhang et al., 2011). PMF model was first introduced by Paatero and Tapper, (1994) as follows:

$$x_{ij} = \sum_{k=1}^{p} g_{ik} \times f_{kj} + e_{ij} \tag{1}$$

where x_{ij} is the elements of the matrices for the measurements, g_{ik} is the factor time series, f_{kj} is the factor profiles, and e_{ij} is the PMF residuals. The subscripts i, j, and k represent time, m/z, and a discrete factor, respectively. The superscript, p represents the number of factors. PMF finds the model solution by using the least-squares algorithm by iteratively minimising the following quantity:

$$Q = \sum_{i=1}^{n} \sum_{j=1}^{m} \left(\frac{e_{ij}}{\sigma_{ij}}\right)^2 \tag{2}$$

where σ_{ij} is the measurement uncertainty.

However, the PMF model does not provide a mathematically unique solution, an issue which is usually referred to as rotational ambiguity (Paatero et al., 2002). Specifically, the model can deliver the identical value of Q for a combination of the matrices **G** (time series) and **F** (factor profiles) and for a combination of their rotations G_- and F_- (with $G_- = G \bullet T$ and $F_- = T^{-1} \bullet F$). In this case, Q is the same, despite the solution being possibly entirely different. Even though the non-negativity constraints limit the number of allowed rotations, there are still many possible rotations and thus solutions. In order to reduce the rotational ambiguity of the PMF model, Paatero and Hopke (2009) proposed a multilinear engine (ME-2) algorithm, which allows the addition of *a priori* information into the model (e.g., source profiles or time series of external data (i.e., data external to the PMF input matrices)) to avoid unrealistic rotations and to generate more unique solutions. Using a priori information allows the user to guide the model towards an environmentally reasonable solution. Canonaco et al. (2013) implemented

an ME-2 solver (Paatero, 1999) into the Igor-based software package, Source Finder (SoFi). SoFi enables the users to have enhanced rotational control over the factor solutions by imposing constraints via, e.g., the *a*-value approach, on one or more elements of **F** and/or **G** (Paatero and Hopke, 2009). For instance, the *a* value (ranging from 0 to 1) is the tolerated relative deviation of a factor profile (f_k) or time series (g_k) from the chosen a priori input profile (F_k) or time series (G_k) during the iterative least-square minimization, as demonstrated in Equations (3a) and (3b) (Canonaco et al., 2013):

$$f_k = F_k \pm a \bullet F_k \tag{3a}$$

$$g_k = G_k \pm a \bullet G_k \tag{3b}$$

2.2. Rolling PMF analysis with bootstrap and random a-value approach

Conventional PMF is conducted over the whole dataset, with the assumption that the OA source profiles are static, which can lead to high errors when it comes to long-term datasets considering that OA chemical fingerprints are expected to vary over time (Paatero et al., 2014). For instance, (Canonaco et al., 2015) showed a substantial seasonal variability of oxygenated organic aerosol (OOA) factor profiles. Parworth et al. (2015) first proposed to run PMF analysis on a smaller time window (e.g., 14 days) to roll over the whole dataset with a certain step. This technique was further refined by Canonaco et al. (2021). The rolling PMF window mechanism allows the PMF model to adapt the temporal variations of the source profiles (e.g., biogenic versus biomass burning influences on OOA), which usually provides well-separated OA factors. In addition, with the help of the bootstrap strategy (Efron, 1979) and the random *a*-value approach, users can estimate the statistical and rotational uncertainties of the PMF results (Canonaco et al., 2021).

2.3. A standardised protocol of SA for a long-term dataset using SoFi pro

This work presents a standardised protocol to identify main OA components. These guidelines work well for all 22 datasets despite the various pollution sources and OA levels at the different stations. All 22 datasets were analysed by following the protocol described in this study to minimise user subjectivity. Fig. S1 provides the general working flow of this protocol, while the more detailed step-by-step guideline is summarised in Table 1. Detailed explanations of each step are unfolded in the following subsections.

2.3.1. Seasonal PMF pre-tests

To effectively implement rolling PMF analysis, knowing potential sources for each season for any given site is crucial. Seasonal PMF *pre-tests* allow us to retrieve reasonable seasonal PMF results (so-called base case). The first step of the *pre-tests* is to conduct unconstrained PMF with varying factors from 2 to 8 for each season. Based on the time series, diel patterns, factor profiles, and correlation with external data, the number of factors for each season could potentially be pre-determined. Examining a solution up to a relatively high number of factors (8 in this case) is crucial as some primary factors (e.g., HOA, BBOA, COA, and CCOA) might only appear in the PMF solution when the number of factors increases. Given the similar chemical fingerprints of some of the primary sources, it is possible that for a low number of factors, they remain mixed (e.g., HOA and COA). In this section, the approach used to identify each source type effectively is covered in the following paragraphs.

For a site potentially impacted by traffic, it is suggested to constrain the HOA mass spectrum using the one from Crippa et al. (2013) with a tight *a* value (0.05–0.1) and a narrower range of factors (3–7). Typically, the HOA factor has a pronounced diel pattern with distinct morning and evening rush hour peaks, and the HOA factor profile is typically similar among different sites (Crippa et al., 2014). However, when the diel pattern does not show the typical variability expected from traffic emissions, one should consider using the HOA mass spectrum from

Table 1
Step-by-step protocol for running rolling PMF.

	Detailed steps
1. **Seasonal PMF** *pre-tests*	1.1. Unconstrained runs (2–8 factors)
	1.2. Test for the presence of OA factors (in order of hydrocarbon-like OA (HOA), biomass burning OA (BBOA), cooking-like OA (COA), coal combustion OA (CCOA), special local factors (if applicable), and OOA factors)
	1.3. Residual analysis (no structural patterns in diel profiles/time series/mass spectra)
	1.4. *a*-value sensitivity analysis for constrained factors (i.e., primary OA factors (POAs))
2. **Seasonal bootstrap analysis**	2.1. Constrain the POAs and site-specific factor(s) in mass spectra retrieved from base case (the satisfactory solutions from seasonal *pre-tests*)
	2.2. Combine the bootstrap resampling strategy with random *a*-values with an upper *a*-value of 0.4–0.5 for POAs and site-specific factor(s) and a repeat of 100–1000 times
	2.3. Use the same technique as mentioned in step 4 (see later) to filter out PMF runs that are not environmentally reasonable
	2.4. Quality check for the bootstrapped solution
3. **Rolling PMF**	3.1. Constrain primary factor MS using published profiles or averaged site-specific profiles from seasonal bootstrapped solutions
	3.2. Constrain site-specific factor MS (if those exist) using random *a*-value approach within a range of 0–0.4 and a step of 0.1. An upper limit of 0.5 for BBOA *a*-value could be considered
	3.3. Enable bootstrap and set the length of the PMF window (7, 14 or 28 days)
	3.4. Set the range of the number of factors based on the number of factors obtained during the seasonal analysis
4. **Criteria-based selection for PMF runs** (Table S2)	4.1. Define a sorting criterion for more oxidised-oxygenated OA (MO-OOA) (f_{44} for the MO-OOA) in case there are two unconstrained OOA factors
	4.2. Selection criteria of PMF solutions based on correlations with external tracers
	4.3. Selection criteria of PMF solutions based on time series (e.g., hours of COA, explained variation of key ions by specific factor)
	4.4. Define the "best" PMF runs using the relevant/ appropriate statistical tests (e.g., *t*-test approach)
	4.5. Optimize time windows (compare non-modelled points and Q/Q_{exp} among different time windows)

unconstrained PMF runs or loosen the *a-value* for HOA from Crippa et al. (2013). When a BBOA-like factor exists in both unconstrained and HOA-constrained runs, the "local" BBOA spectrum retrieved from these runs are recommended to be used as a constraint/reference profile in the next step of the PMF analysis. This is because of the relatively large spatial variabilities of BBOA factor profiles (Crippa et al., 2014). The expected BBOA factor usually has a pronounced contribution of *m/z* 29, 60, and 73 signals and a distinct diel pattern with high concentration during nighttime. If the BBOA factor was not present in previous steps, it should be checked if f_{60} (i.e., the fraction of *m/z* 60 to the total organic mass) is above the background level of 0.3% (Cubison et al., 2011), and also has a clear temporal pattern beyond the noise. However, f_{60} should not be the only criterion to determine the existence of BBOA (the background level of f_{60} is instrument-dependent). Constrained PMF runs with a reference BBOA spectrum (Crippa et al., 2013; Ng et al., 2011a) and a relatively high *a*-value (0.3–0.5) need to be performed to seek more proof of its existence by (i) comparing the solution without a BBOA factor; (ii) by checking the correlation factor between HOA vs eBC$_{ff}$, BBOA vs eBC$_{wb}$; and (HOA + BBOA) vs eBC$_{total}$; (iii) by checking if the solution has smaller scaled residuals of *m/z* 60, etc. One should keep in mind that the model performance metrics should determine the choice of reference BBOA profile.

If different slopes in f_{55} vs f_{57} plots at different hours of the day point

towards the presence of COA (Mohr et al., 2012), it should be constrained tightly using the corresponding spectrum from Crippa et al. (2013) with an *a* value of 0.05–0.1. Then, it should be checked if the diel pattern (mass concentration or mass fraction) is reasonable, i.e., it peaks during the time of expected cooking-related activities (noon/afternoon and evening peaks). The COA factor is typically only present in urban environments close to residential and commercial areas.

For an environment with potential coal combustion sources, looking for a "local" CCOA factor mass spectrum from unconstrained or HOA-constrained PMF runs is recommended. However, it is typically challenging to identify the CCOA factor with ACSM data when its contribution is not significant because of the relatively low *m/z* resolution and since the mass range (up to 100/120 for Q-ACSM) does not include polyaromatic hydrocarbons (PAHs). In addition, the similar spectral pattern of hydrocarbon ions (e.g., $C_nH_{2n-1}^+$ and $C_nH_{2n+1}^+$) between HOA, BBOA and CCOA makes it challenging for PMF to resolve these two factors (Sun et al., 2016). Therefore, the existence of CCOA should be justified at least by the most significant contribution of *m/z* 115 (mainly $C_9H_7^+$) and the absence of the morning rush hour peak.

Sometimes, PMF can also help picking up a site-specific factor with special fingerprints in previous steps (besides some common primary organic aerosols (POAs) and OOAs). In that case, the key ions should be checked to investigate potential sources, then the fragmentation table to understand how these key ions are calculated. Most importantly, OOA components should not be constrained as they are expected to vary season by season due to different precursor sources and oxidation capacity of the atmosphere. Typically, more and less oxidised-oxygenated OA (MO-OOA and LO-OOA, respectively) are found within the unconstrained factor(s). Here, the MO-OOA and low volatility oxygenated OA (LV-OOA) are interchangeable. The same applies to LO-OOA and semi volatile-oxygenated OA (SV-OOA). But we refer to these two OOA factors as MO-OOA and LO-OOA in the rest of the text. However, a static number of OOA factors for different seasons is highly recommended if it is environmentally reasonable since it remains challenging to objectively justify the exact transition period for the different number of factors at different periods.

Scaled residuals should be monitored throughout the PMF analysis. Structure in the scaled residuals' daily cycle might indicate missing or incompletely separated sources. In addition, spikes and structural patterns in the time series of the scaled residuals always require extra attention, as they suggest some high uncertainties of the current model for these points/periods or instrument issues. Also, if the constrained profiles cause systematic patterns in the residuals, they should be reconsidered or tested with a larger *a* value. Last but not least, the *a*-value sensitivity analysis for constrained factors should be conducted to optimise (i.e., towards enhanced correlation with externals, reasonable factor profiles, and small scaled residual, etc.) the constrained factor to the dataset of interest. Then, once the reasonable PMF solution has been determined (so-called base case result), the mass spectra for all constrained factors are used as input factors for bootstrap analysis in the next step.

2.3.2. Seasonal bootstrap analysis

A bootstrap resampling strategy (Efron, 1979) is recommended to test the stability of the base case solutions. Therefore, all the mass spectra of constrained factors (i.e., POAs and site-specific factors) should be constrained using the random *a*-value technique (Canonaco et al., 2021; Chen et al., 2021) with an upper *a* value of 0.4–0.5 and repeats of 100–1000. Next, the same technique mentioned in Section 2.3.4 should be used to filter out "incorrect" (not environmentally reasonable) solutions. As a next step, the quality of the averaged solution of selected PMF runs should be checked in terms of the uncertainties of factor profiles, time series, and percentage of selected runs. If the bootstrap solution shows significant uncertainties, the base case needs to be re-evaluated. The mass spectra for all constrained factors resulting from the bootstrap phase should be saved and used for rolling PMF analysis in the

next step.

2.3.3. Rolling PMF

The mass spectra from bootstrapped solutions are recommended as the reference profiles to constrain POA and site-specific factors during rolling PMF. BBOA is known as the most spatiotemporally variable factor compared to all other POA factors (Crippa et al., 2014). Also, considering that the highest mass concentrations of BBOA occur in winter, the BBOA mass spectrum from the bootstrapped winter solution is recommended as the constraint, as it is more representative of the dataset. Alternatively, the published profiles (HOA and COA from Crippa et al. (2013) and BBOA from Ng et al. (2011a) or Crippa et al. (2013)) could be used (Canonaco et al., 2021). Canonaco et al. (2021) suggested using a random a-value technique (randomly select a values for each constraint within a certain range) and bootstrap resampling strategy to estimate the rotational uncertainties of rolling PMF. Based on the seasonal bootstrap analysis, the upper a value for the site-specific factors can be determined by the seasonal variation and uncertainties. Canonaco et al. (2021) showed that an upper value of 0.4 for POAs is sufficient to cover the temporal variabilities. However, an upper a value of 0.5 for BBOA is suggested when high temporal variabilities of the BBOA mass spectrum are expected. When the number of factors is not identical for all the seasons, the rolling PMF should be conducted with both n and $n + 1$ factors over the entire dataset.

2.3.4. Criteria-based selection for PMF runs

With the large number of PMF runs expected for rolling analysis (e. g., >15,000 runs for a one-year dataset with 30-min time-resolution), inspecting each single PMF run is not feasible. Therefore, a criteria-based selection should be used to (i) evaluate the quality of the PMF runs quantitatively and relatively objectively and (ii) sort out the unconstrained factors in the same order for further averaging. The criteria-based selection has been explicitly explained in Canonaco et al. (2021). In short, SoFi Pro enables the user to define criteria based on the time series and/or factor profiles to select environmentally reasonable solutions. In addition, this criteria-based selection function can also serve to reposition unconstrained factors as unconstrained factors can appear in random order in a different iteration of the PMF. The inexact sorting criteria can result in a mixing of the unconstrained factors. Therefore, it is crucial to use the most representative sorting criterion, i.e., f_{44} for the MO-OOA (criterion #7 in Table S2), as suggested by Chen et al. (2021). At the same time, it is also recommended to monitor f_{44} in MO-OOA and f_{43} in LO-OOA to reject zero-values of these two criteria. The criterion of f_{44}/f_{43} for MO-OOA is not recommended because it could accept PMF solutions with smaller f_{44} in MO-OOA than LO-OOA when f_{43} is extremely small. Statistical tests such as the t-test (Chen et al., 2021) for time series based criteria (#4, #5 and #7 in Table S2) and correlation-based criteria (#1, #2 and #3 in Table S2) should be performed to minimise subjective decisions. With a p value ≤ 0.05, it is possible to select PMF runs with statistically significantly higher scores compared to the same criterion for other factors (for time series based criteria) or statistically higher correlation with each other (for correlation-based criteria). This technique allows the user to select environmentally reasonable PMF solutions with minimal subjective judgements. Last but not least, the optimum length of the time window should be determined by minimising non-modelled data points and Q/Q_{exp} while applying the same criteria and thresholds to these PMF runs with different time windows (7, 14 or 28 days) (Canonaco et al., 2021; Chen et al., 2021). Based on our study, a 14-day window size is the most commonly selected one, which is consistent with previous studies (Canonaco et al., 2021; Chen et al., 2021).

2.3.5. Special cases and limitations of the current protocol

For all the 22 ACSM/AMS datasets, this standardised protocol works well in general. However, different numbers of factors at different periods remain challenging for rolling PMF. There are three special cases

that this protocol could not cover. Specifically, the BBOA factor is not present in the warm period for the Barcelona, Cyprus, and Marseille datasets. However, this protocol could not cover such situations with a proper criterion to objectively include/exclude certain OA factors (e.g., BBOA) in certain time periods. The distribution of the correlation between BBOA and eBC_{wb} was utilised for the Marseille data, which appears to have a bimodal Fisher distribution. Thus, the 10th percentile results from the separated distributions were used as thresholds to define the existence of BBOA (Chazeau et al., 2022). For the Barcelona and Cyprus datasets, the criterion to decide the existence of BBOA is the explained variation of f_{60} by BBOA. A t-test was conducted with the null hypothesis that the variation of f_{60} explained by BBOA is not significantly larger than that of other factors. The presence of BBOA is only considered when the p value was ≤ 0.05. In addition, as discussed before, a different number of factors often suffers from more uncertainties at the edge of the transition period by averaging different numbers of factor solutions simultaneously. One strategy to avoid averaging over different numbers of factor solutions is to unselect any data point in a range of $edge \pm window\ length/2$. However, it could potentially lead to relatively more non-modelled points during the transition period. Therefore, keeping a static number of factors in the rolling analysis as much as possible is recommended if that is environmentally feasible. Thus, it remains challenging to objectively define the transition point to an improved source apportionment for rolling PMF analysis with a different number of OA factors.

3. Results and discussions

Figure 2 provides an overview of the mean OA mass fractions and their main components at 22 stations across Europe. Overall, the total PM_1 (sum of OA, eBC, nitrate (NO_3), sulfate (SO_4), ammonium (NH_4), and chloride (Chl)) mass concentration has an average of 9.7 ± 7.9 μg/ m^3, with generally higher concentrations at urban stations (brown circles, avg = 12.2 ± 9.3 μg/m^3) compared to non-urban ones (green circles, avg = 6.2 ± 3.3 μg/m^3). Kraków is the most polluted site (40.4 μg/ m^3), and Birkenes is the cleanest (1.3 μg/m^3). The OA contribution to the total submicron aerosol ranges from 21 to 75%, which is consistent with previous results based on shorter campaigns (Jimenez et al., 2009). For other main chemical species, eBC, NO_3, SO_4, NH_4, and Chl exhibit an average contribution to the total PM_1 of 10.0%, 15.0%, 16.2%, 9.9% and 1.2%, respectively. eBC and NO_3 show higher contributions at the urban sites (12.1% and 16.2%) than at the non-urban ones (6.8% and 13.3%).

3.1. Overview of the primary and secondary OA

Primary and secondary OA factors are identified for each station in Fig. 2. In this study, all the OA factors except MO-OOA and LO-OOA are considered as POA factors. Overall, the well-known POA factors have been resolved, including HOA and BBOA. All datasets identify HOA except Hyytiälä (non-urban). BBOA is resolved in 19 datasets (12 urban and 7 non-urban sites) with the exceptions being Hyytiälä, Puy de Dôme, and Helsinki. In general, both HOA and BBOA present considerable fractions of the total submicron aerosol with average contributions of 5.0% and 5.6%, respectively. Also, they both show higher contributions at the urban sites (HOA: 5.7% and BBOA: 6.3%) than at the non-urban ones (HOA: 4.0% and BBOA 4.5%). COA is identified in three southern European cities (i.e., Athens, Marseille, and Barcelona), a megacity (London), and a central European city (Zürich). It has an average contribution to the total PM_1 of 6.3%. CCOA is resolved in Kraków (Tobler et al., 2021) and Melpitz (non-urban) with contributions of 5.8% and 6.9%, respectively. SFOA, which likely originates from peat and coal combustion, appears at the two Irish sites (Dublin (urban) and Carnsore Point (non-urban)), with contributions of 12.2% and 6.0%, respectively. In addition, local factors (i.e., specific to a single monitoring site) are highlighted in this study: an m/z 58-related OA (58-OA) in Magadino (1.2%); a coffee roaster OA factor in Helsinki (3.0%); a sea salt factor at
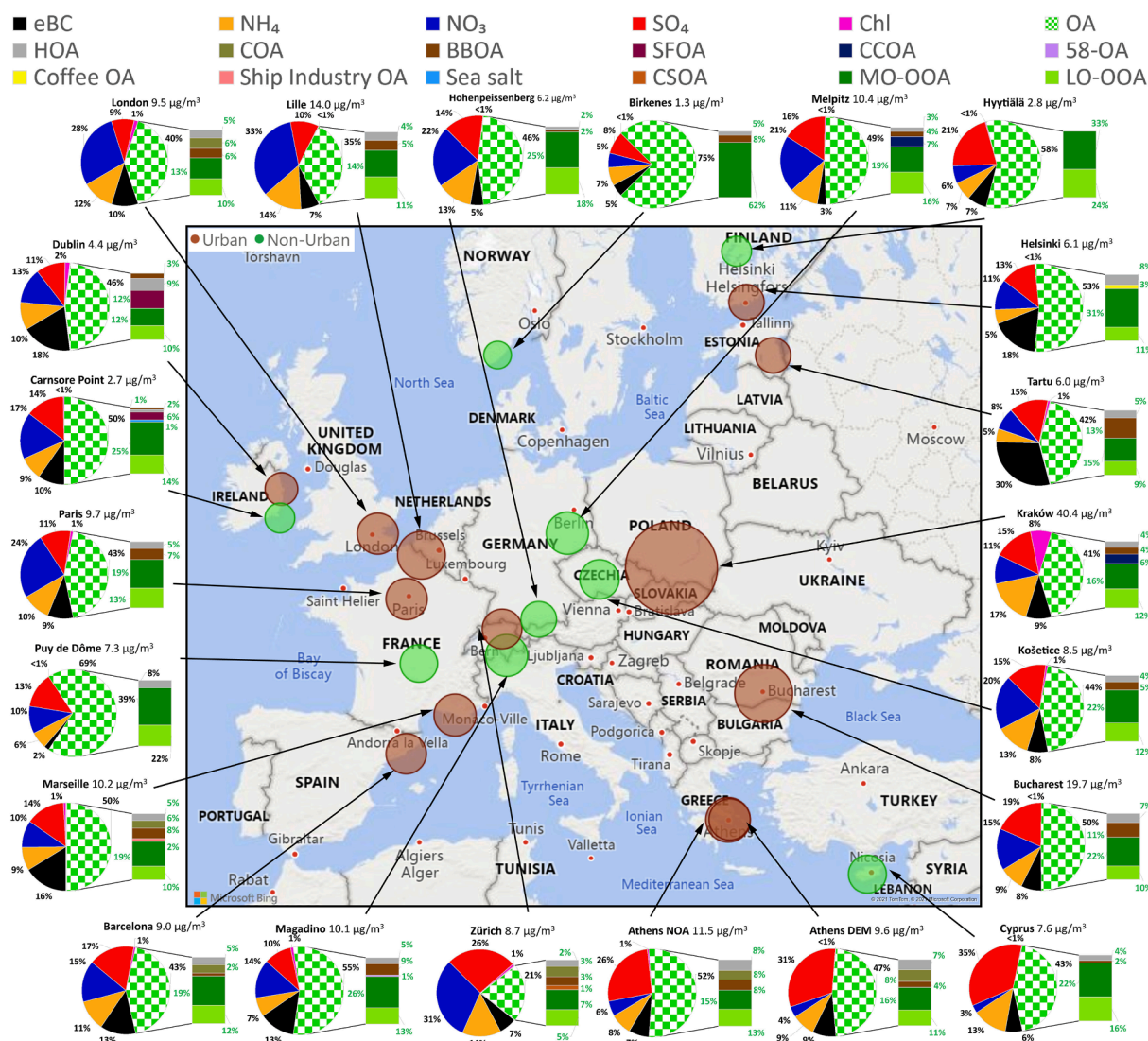
Fig. 2. Submicron particulate matter (PM$_1$) mass concentration (in μg/m^3) and mass fractions of non-refractory inorganic species, equivalent black carbon (measured by online filter-based methods), and organic aerosol measured with the 22 ACSM/AMS at multiple locations in Europe covering all seasons. The size of the markers corresponds to the PM$_1$ mass concentration. The brown colour of the marker indicates an urban site, while the green marker indicates a non-urban site. The checkered green/white shading of the pie charts denotes the organic aerosol (OA) fraction in PM$_1$, and the bar charts represent the contributions of each OA factor to the total OA mass.

Carnsore Point (1.5%); cigarette smoking OA (CSOA) in Zürich (Qi et al., 2019; Stefenelli et al., 2019); and a mixed ship-industry factor in Marseille (2.2%, Chazeau et al., 2022). Finally, two secondary OOA factors (MO-OOA and LO-OOA) are present at all sites except for Birkenes (MO-OOA only). The MO-OOA and LO-OOA contribute to the total PM$_1$ with an average of 22.0% and 13.1%, respectively. Both MO-OOA and LO-OOA show drastic differences among urban (16.7% and 10.6%) and non-urban sites (29.6% and 17.2%), which is expected since more primary sources are present in the urban environment. When summing up MO-OOA and LO-OOA (Total OOA), Fig. 2 suggests that secondary OA is the main contributor to total submicron PM (average = 34.5%, range from 11.7 to 62.4%) and dominates OA (average = 71.1%, range from 47.3 to 100%) across Europe.

In addition, the resolved OA factors have been validated using data external to the PMF input matrices as well as the mass conc. of *m/z* 60 in the organic matrix (Table S4). These external data include NH$_4$, NO$_3$, SO$_4$, which were obtained from ACSM/AMS, and eBC was measured by AE33/AE31/MAAP. Regarding the PMF errors (Equation (6) in Canonaco et al. (2021)), they are estimated by logarithmic probability density

functions (pdf) of the standard deviations of each time point *i* divided by the mean concentration of each time point *i* for corresponding OA factors. The PMF errors of major OA components are presented in Table S6. In general, POAs often have smaller PMF errors than OOA factors since they are always constrained.

3.2. OA composition changes as a function of OA loading

To understand how the OA composition changes under different loadings, each dataset is divided into ten bins containing the same number of points based on the OA mass concentrations. As shown in Fig. 3, apart from Zürich and Helsinki, all urban as well as two non-urban sites (Magadino and Melpitz) report larger POA contributions under high OA loadings. It is most likely because primary emissions substantially contribute to OA mass concentrations in relatively polluted areas under stagnant conditions (Tobler et al., 2021; Zhang et al., 2019). Specifically, HOA shows a relatively constant contribution even when the OA mass concentration increases at non-urban sites, while it increases as the OA mass concentration increases at urban sites. This
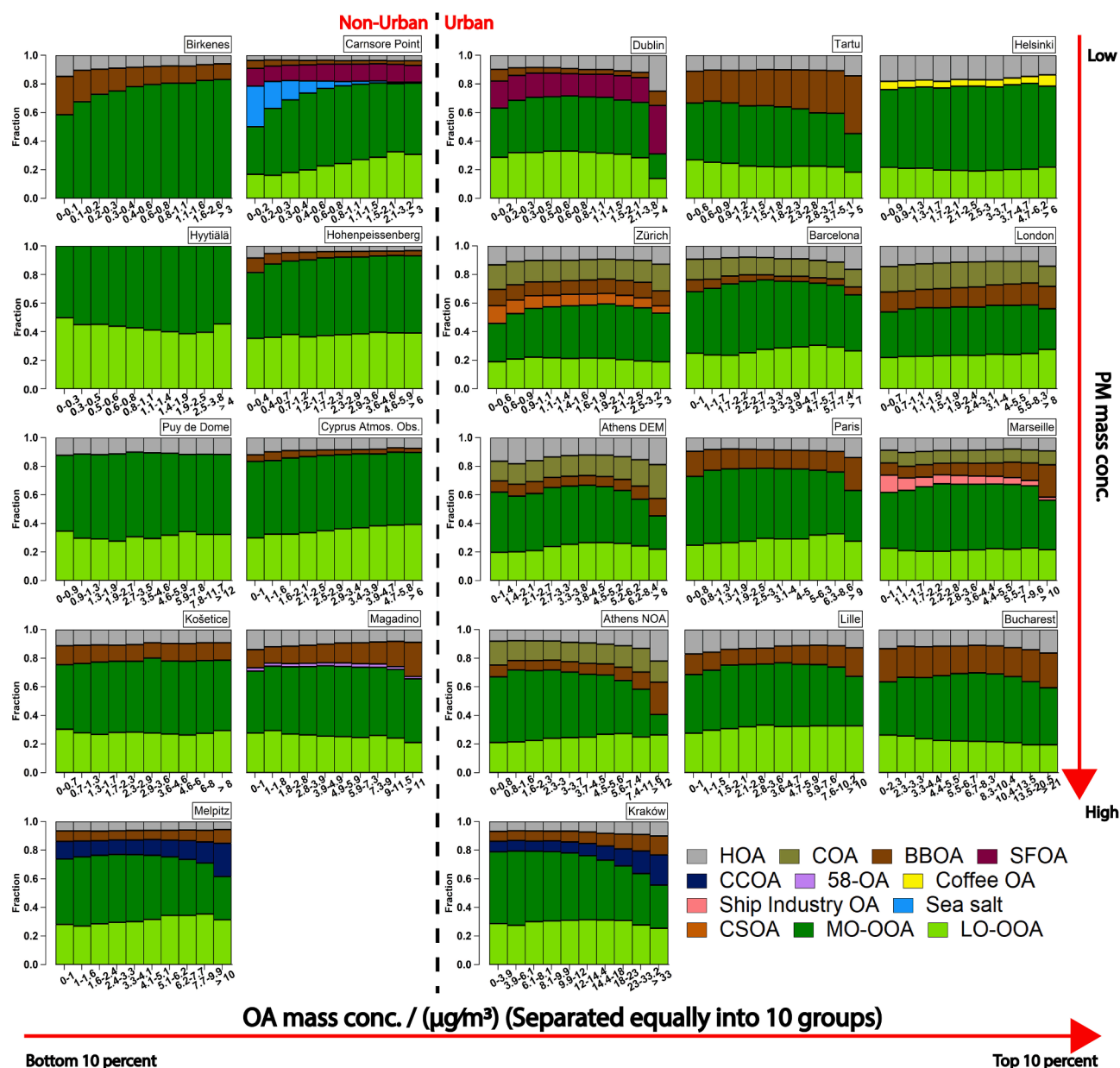
Fig. 3. Mass fraction of each organic aerosol (OA) component for 22 stations with 10 equally distributed bins based on OA mass concentration. Non-urban and urban sites have been separated by the dashed vertical line divided into left and right panels. The sites are sorted based on the submicron total particulate matter (PM$_1$) mass concentration. In general, oxygenated OA (OOA, dark and light green bars) is dominant at all sites over the whole mass range. However, with an increase of the total OA mass concentration, an increase in the primary OA fraction is often observed.

suggests that traffic emissions still play a considerable role during high OA mass concentration periods, and it remains important even when the total OA mass concentration is low. In particular, all factors related to the combustion of solid fuel (i.e., BBOA, SFOA, and CCOA) show the most pronounced enhancement when the OA mass loading increases, especially during winter seasons (Fig. S3 in the Supplement), which suggests solid fuel combustion is the main driver for the polluted episodes. The sea salt factor at Carnsore Point, in turn, has the highest contribution in the bottom 10 percent of OA mass loadings since high wind speeds favour high sea salt emissions and low OA mass concentrations at the same time.

3.3. Diel cycles for resolved OA components

The highly time-resolved long-term ACSM/AMS data allow investigating the diel cycles of the OA components. Figure 4 shows the averages

(solid lines) and standard deviations (shaded areas) of diel profiles of the major OA components (HOA, BBOA, COA-like, MO-OOA, LO-OOA and Total OOA), normalised by the annual average of the corresponding OA component mass concentration for each site at both non-urban and urban sites. Birkenes and Hyytiälä datasets are not included because they only have 4-hour and 3-hour time resolutions, respectively. Overall, all OA components exhibit increases during the evening since accumulation occurs in a shallow boundary layer during that time of the day. However, the decreasing trends from midnight to sunrise are caused by decreased emissions and relatively higher wind speed, and the dilution of OA components after sunrise is caused by the rising boundary layer which introduces clean airmasses (Stull, 1988).

HOA shows a distinct pattern at urban sites with characteristic morning and evening rush-hour peaks. By contrast, at non-urban locations, HOA does not follow the same pattern, indicating that this factor is likely associated with transported traffic emissions or with non-traffic
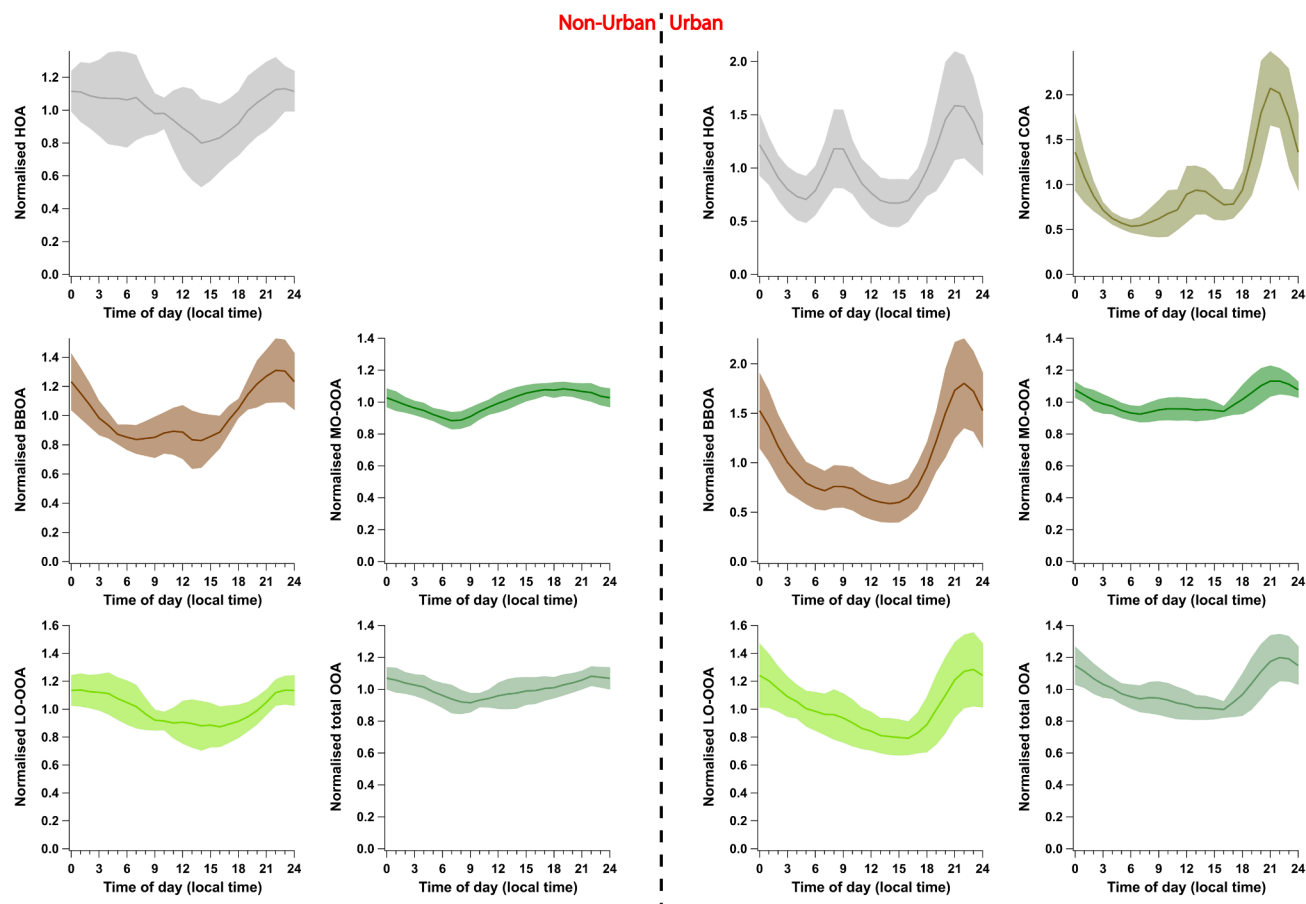
Fig. 4. Normalised diel profiles for HOA, COA, BBOA, MO-OOA, LO-OOA, and Total OOA (MO-OOA + LO-OOA). The solid lines and shaded areas represent the averages and standard deviations, respectively, of the diel profiles for the non-urban and urban datasets (normalised by the annual average of the corresponding OA component mass concentration for each site). The POA factors generally show more pronounced variability than the OOA factors. In addition, the urban sites have stronger patterns with less spatial variability than the non-urban sites.

primary hydrocarbon emissions at these sites. COA, as mentioned resolved at six urban sites, shows distinct noon and evening peaks with minor standard deviations, which suggests small spatial variabilities of cooking emissions. BBOA has a similar diel cycle at urban and non-urban sites with reduced values during the day and a marked evening peak, which indicates that most likely, (residential) heating emissions are the main contributor to BBOA. However, at the urban sites, the evening peak of BBOA is more pronounced than at the non-urban sites, which suggests that the urban BBOA is more local and synchronised to domestic heating than at the non-urban sites. The delayed morning peaks and broader span of non-urban BBOA diel profiles further indicate relatively distant BBOA sources at non-urban sites.

The MO-OOA diel trend at both urban and non-urban sites shows the most stable pattern. A slight decrease is observed during the night starting after 23:00 and continuing until 06:00–07:00, probably due to the decrease in the formation rates of MO-OOA in the absence of photochemical activity. By contrast, the MO-OOA concentrations increase slightly from morning to afternoon at the non-urban sites, potentially due to photochemistry. Moreover, the long-range transported origin could also play a role in this stable diel trend of MO-OOA. The enhancement of MO-OOA after 18:00 at urban sites is due to the accumulation of pollutants in a shallow boundary layer. This includes both OOA precursors and POA, both of which may be oxidized by OH or NO₃ radicals. The diel cycles of LO-OOA at the urban and non-urban sites reveal nighttime maxima with a slight decrease at noon, suggesting local production or enhanced vapour partitioning onto pre-existing aerosol in the shallow nocturnal boundary layer. Urban LO-OOA shows much stronger evening peaks than at non-urban sites,

potentially caused by nighttime chemistry yielding urban OOA from POA oxidation (where POA includes both HOA, BBOA, and other primary sources). Kodros et al. (2020) and Tiitta et al. (2016) demonstrated how dark ageing of BBOA could potentially yield substantial amounts of OOA. Such ageing is likely to explain some of our observations at the urban sites (Zhang et al., 2020). Both urban and non-urban sites show small spatial variability for the Total OOA, but the diel cycle for urban sites has a more substantial evening peak again due to the strong LO-OOA increase. In general, the POA factors show more temporal variability than the OOA factors at both urban and non-urban sites.

In addition, Fig. S5 shows the averages of normalized weekly cycles for the non-urban and urban sites separately (with Birkenes and Hyytiälä datasets included among the non-urban sites). Each weekly cycle has been normalised by the annual average of the corresponding OA component mass concentration for each site. Compared with the diel cycles, the weekly ones are generally much weaker. In addition, POA shows a stronger variability compared to the OOA factors, similar to the averaged diel cycles (Fig. 4). HOA shows lower values during the weekend than on weekdays at both urban (-2.6%) and non-urban (-3.5%) sites. Except for HOA, the non-urban weekly cycles are much less pronounced than the ones at the urban sites. Specifically, BBOA increases during the weekend, with 19.9% and 12.3% higher values than on the weekdays for urban and non-urban sites, respectively. This is because more wood-burning activities (e.g., open fire grills and residential heating) are expected during weekends (Fuller et al., 2014). COA shows a similar trend as it increases during the weekends (+18.8% at urban sites), suggesting that cooking activities are more pronounced. All OOA factors (MO-OOA, LO-OOA, and Total OOA) do not present strong

weekly cycles (<6.3% difference between the weekdays and the week-end), with relatively larger spatial variability for OOA at the urban sites, indicated by larger standard deviations.

3.4. Spatial and seasonal variability of OA contributions

The time series of daily-averaged OA fractions for each site is shown in Fig. S2, which presents an overall picture of the entire source apportionment result. It indicates significant spatial and temporal variabilities of OA contributions across Europe. To study the seasonal variation of OA and its sources, data was divided into four seasons: winter (DJF: December, January, and February), spring (MAM: March, April, and May), summer (JJA: June, July, and August), and autumn (SON: September, October, and November). Figure 5 indicates a relatively small spatial variability of the relative OA contributions at both urban and non-urban datasets, and there is no clear pattern between the OA fraction and PM$_1$ loading. Urban sites have higher POA contributions in OA than non-urban sites. However, each dataset shows an apparent seasonal variability with higher POA contributions and mass concentrations in cold seasons than in warm ones (Fig. 5 and Fig. S6). The contributions of POA also appear to be higher when the total PM$_1$ mass concentration increases at all non-urban sites, as shown in Fig. 5.

Specifically, urban sites show higher HOA contributions (overall average contribution of 12.7 ± 2.9%) than non-urban sites (7.4 ± 2.7%), which is expected due to more traffic emissions in urban areas. Moreover, for both urban and non-urban sites, the HOA contribution shows a distinct seasonality with the lowest contribution in summer (8.8 ± 3.4%) and the highest in winter (12.0 ± 4.8%), and similar

contributions in spring (10.9 ± 4.3%) and autumn (11.5 ± 4.6%). This might be due to the lower boundary layer with stagnant conditions in the cold season favouring the accumulation of primary and local pollutants and/or reduced photochemistry. In addition, the heating-related sources (i.e., BBOA, CCOA, and SFOA) are obviously more pronounced during the cold seasons than the warm ones. Specifically, BBOA has an average contribution of 8.3 ± 4.7% in summer but 16.9 ± 8.4% in winter. CCOA was only found in Kraków and Melpitz, and its contributions varied from season to season, with substantially enhanced contribution during winter (Kraków: 18.2% and Melpitz: 23.1%) compared to summer (Kraków: 4.5% and Melpitz: 8.7%). The drastic seasonal variations in Kraków are due to the widespread use of coal-burning for residential heating purposes in winter (note that these measurements took place before the government imposed a ban on the use of solid fuels for residential heating in the city of Krakow (Casotto et al., 2022; Tobler et al., 2021)). In Melpitz, coal combustion is less dependent on local sources, but likely more affected by emissions from Poland or other eastern European countries that are rapidly transported by advection in winter, leading to the observed seasonality. For the Dublin dataset, the SFOA (heavily affected by both peat and coal combustion sources (Lin et al., 2019, 2018)) shows an enhanced contribution in winter (32.9%) and a decreased contribution in summer (13.2%). The SFOA in Carnsore Point station shows less seasonality because of the absence of local sources but still has a higher contribution in winter (13.3%) than in summer (9.2%). The COA contribution shows almost no seasonality, ranging from 14.3 ± 2.7% in summer to 15.4 ± 3.3% in autumn at the six urban sites where this factor is resolved, suggesting that the cooking emission contribution is constant and non-negligible in
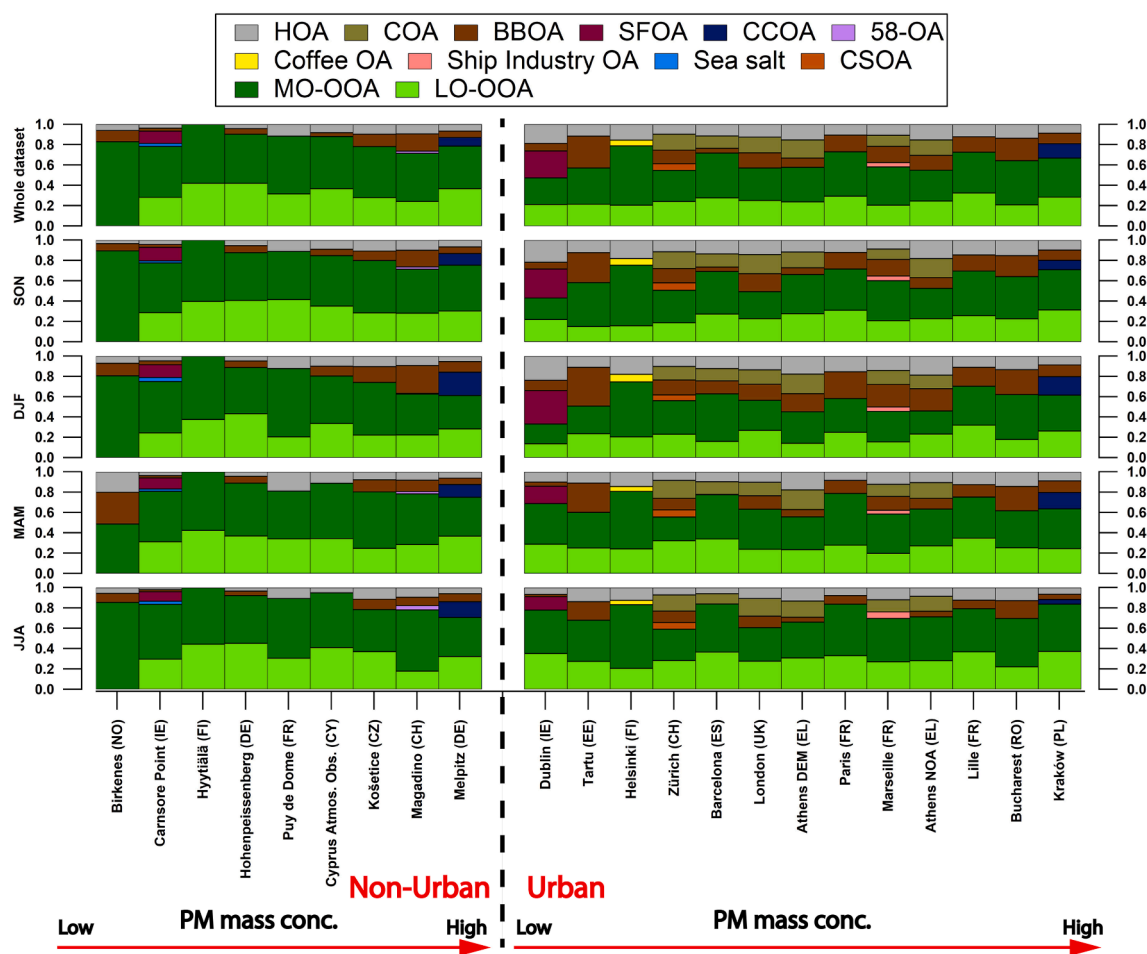
Fig. 5. Relative contributions of all OA components at each station grouped by season (see text). The stations are categorised into non-urban (left) and urban sites (right), where each subset is ordered by PM$_1$ mass concentration.

European cities in all seasons. The specific contributions of all OA components for all datasets and all seasons are summarised in Table S6, in which all POA except HOA, BBOA and COA are summed up as "other OA".

3.5. Spatial and seasonal variabilities of f_{44} vs f_{43} in the OOA factors

Canonaco et al. (2015) analysed the seasonal variability of major ion intensities (i.e., m/z 44 and m/z 43) in the OOA factors in Zürich. They suggested that biomass burning emissions, the most important precursor of SOA in that city during winter, cause the LO-OOA factor to be at the left half of the triangular region shown by (Ng et al., 2010) within the f_{44} vs f_{43} space, consistent with biomass burning emissions as shown by Heringa et al. (2011). In contrast, biogenic SOA from terpene oxidation may "push" the LO-OOA factors to the right side of the triangle in summer (Pfaffenberger et al., 2013).

This study explores the seasonality of f_{44} vs f_{43} for MO-OOA, LO-OOA and the Total OOA factors for both seasons at all sites, as shown in Fig. 6. It shows that the rolling PMF provides a good separation between MO-OOA and LO-OOA in both winter and summer (Fig. 6a), which is consistent with what Canonaco et al. (2021) and Chen et al. (2021) reported for two Swiss datasets. However, the positions of MO-OOA for the different stations in the f_{44} vs f_{43} space show large spatial variability (Fig. 6a), mainly attributed to the complex and various ageing processes in different locations under different meteorological conditions. In general, all LO-OOAs during the summer (JJA) shift to the right side of

the triangle by a different extent when compared to the winter (DJF) seasons (Fig. 6a), which is most likely due to the enhanced biogenic emissions with higher temperatures during summer seasons (Canonaco et al., 2015). The right-side shift from summer to winter is more apparent when summing up the LO-OOA and MO-OOA into the Total OOA factors (Fig. 6b).

At the same time, some site-specific ions could significantly influence the LO-OOA position. For instance, due to the pronounced biomass burning influence in Bucharest during summer, the LO-OOA factor has considerable contributions of m/z 55, 57, 60 and 73, which is accompanied by a low f_{43} in LO-OOA during summer. The LO-OOA factors of the Tartu and Hyytiälä datasets stay on the right side of the triangle even during the winter season. Tartu appears to have a significant BBOA contribution throughout the year (18.2% in summer). Considering biomass burning OA oxidises rapidly, the biomass burning influence is more pronounced in the MO-OOA factor than in the LO-OOA factor during the whole year. That is why the LO-OOA factor in winter remains on the right side of the triangle. Hyytiälä is located in the boreal forest with high biogenic SOA formation in summer (Heikkinen et al., 2021; Yli-Juuti et al., 2021), which explains the high f_{43} in summer. In addition, no POA factors were deconvolved from this dataset following the presented protocol. By utilizing machine learning techniques, Heikkinen et al. (2021) resolved a slightly aged POA factor that could neither be further separated into HOA nor BBOA. This factor appeared only in winter and coincided with a LO-OOA drop to near-zero loadings when utilizing k-mean clustering approach (Heikkinen et al., 2021).
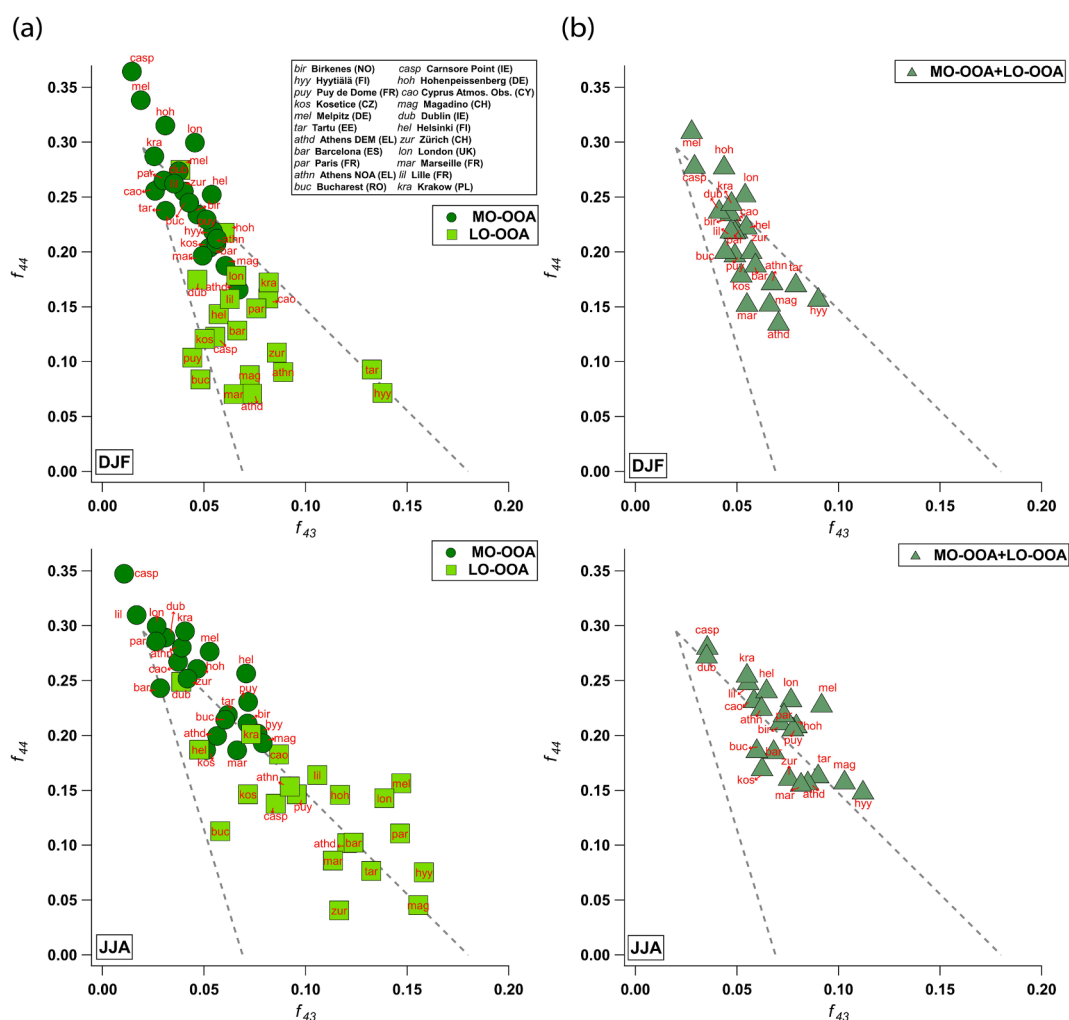
Fig. 6. (a) f_{44} vs f_{43} intensity in (top) winter and (bottom) summer for (a) resolved MO-OOA (dark green) and LO-OOA (light green); (b) the Total OOA (MO-OOA + LO-OOA).

Therefore, it is very likely that the Hyytiälä LO-OOA shown in this study is influenced by aged POA in winter, which keeps the LO-OOA f_{43} high. Also, the potential terpene emission from the Korkeakoski sawmills (ca. 7 km NE of the monitoring station) could also keep the LO-OOA on the right side (Äijälä et al., 2017). The combined effects of high summertime biogenic SOA contribution to LO-OOA and wintertime POA mixing to LO-OOA could explain why LO-OOA in Hyytiälä always stays on the right side of the triangle. When considering the rest of the sites, both the LO-OOA and Total OOA factors generally shift to the right side of the triangle during summer compared to winter.

3.6. Spatial and temporal variabilities of key ions in resolved OA factors

This study also investigates key ions' spatial and monthly variabilities in common OA factors (i.e., m/z 55 and m/z 57 for HOA and COA; m/z 60 and m/z 73 for BBOA; m/z 44 and m/z 43 for MO-OOA, LO-OOA, and the Total OOA). All monthly intensities of these key ions in these OA

factors were averaged across the 22 datasets to see possible monthly trends (Fig. 7). Overall, the key ions for HOA, COA, MO-OOA and Total OOA factors barely show a monthly trend. In contrast, f_{60} and f_{73} in BBOA are substantially higher in the cold months compared to the warmer months. The main reason is likely that levoglucosan and thus m/z 60 is less stable in the aerosol with higher temperature as well as the change in the biomass burning source during different seasons (e.g., residential heating and outdoor open fire) (Bertrand et al., 2018; Bougiatioti et al., 2014; Xie et al., 2014). The most dominating ions (m/z 44 and m/z 43) in the LO-OOA factor show a relatively strong monthly trend compared with MO-OOA and Total OOA. Specifically, f_{44} is smaller, and f_{43} is higher in LO-OOA during the warm months, which is a further indication that the enhancement of biogenically-formed SOA could increase the intensity of f_{43} in LO-OOA when the temperature is increased (which eventually "pushes" the LO-OOA factors to the right side of the triangle as presented in Fig. 6, (Canonaco et al., 2015)). Monthly trends of these key ions of these OA factors for each station are
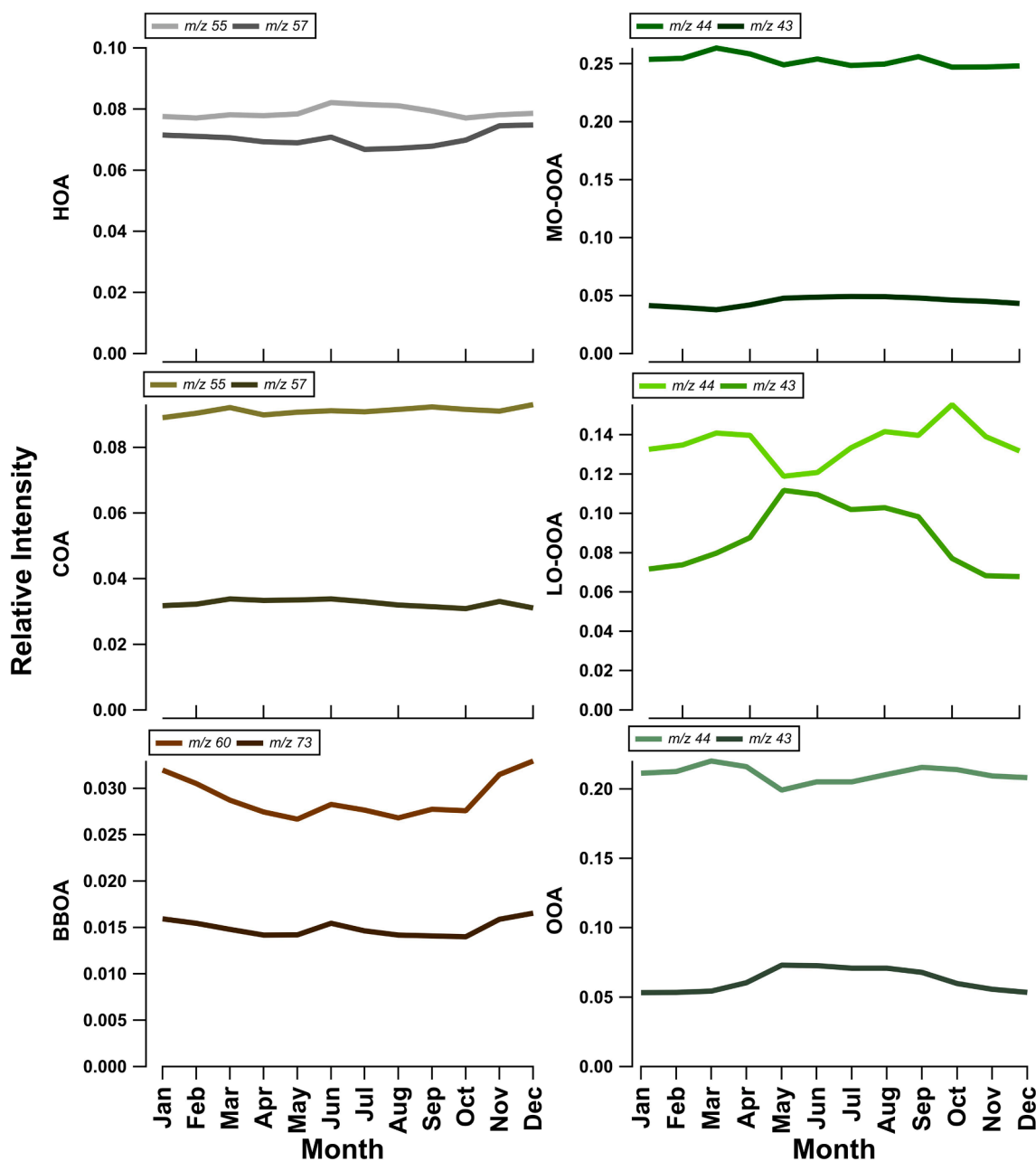
Fig. 7. Monthly average relative intensities of key ions in the corresponding factor profiles over all the datasets.

shown in Fig. S6.

In order to compare the spatial variations of key ions in the different OA factors, the interquartile range (IQR) of the monthly site-averaged intensities was normalised by their median (Table 2). In general, f_{55} for HOA and COA shows a relatively small IQR/median ratio with averages of 0.15 ± 0.03 and 0.16 ± 0.07, respectively. The f_{57} for HOA and COA shows similar consistency across 22 sites with averages of 0.20 ± 0.03 and 0.09 ± 0.05, respectively. Overall, the HOA and COA factors are generally consistent across different locations. It agrees well with the previous findings reported by Crippa et al. (2014). However, the most essential fingerprint ions of BBOA, f_{60} and f_{73}, appear to have the largest spatial variability among the POA factors with IQR/median ratios in a range of 0.28–0.39 and 0.20–0.36, respectively. This is expected since the type of wood and burning conditions, as well as chemical ageing, can affect the BBOA mass spectrum considerably (Bertrand et al., 2018; Bougiatioti et al., 2014; Grieshop et al., 2009; Heringa et al., 2011; Weimer et al., 2008; Xie et al., 2014). Thus, as discussed previously, retrieving site-specific BBOA factor profiles using unconstrained PMF analysis instead of published BBOA factor profiles is strongly recommended.

The most dominating ion in MO-OOA, f_{44}, has a somewhat smaller IQR/median ratio, ranging from 0.16 to 0.34, and the f_{43} in MO-OOA has an IQR/median ratio in a range of 0.45–0.83. This is because different datasets could have significantly variable ageing processes, precursors, and meteorological conditions, which appear to affect the degrees of oxygenation (the relative intensities of m/z 44 and m/z 43). In addition, MO-OOA remains dominated mainly by f_{44} (average $f_{44} = 0.25$), but with a much smaller f_{43} intensity (average $f_{43} = 0.04$). Therefore, the slight changes in the intensity of f_{43} could have a larger effect on the IQR/median ratio for this ion.

Due to enhanced biogenic emissions, the f_{43} in LO-OOA shows consistently larger intensities in the warmer months (May-September), as shown in Fig. 7. Consequently, the f_{44} in LO-OOA decreases during the warm seasons and is related to the seasonal differences in f_{44} vs f_{43} of Fig. 7. In addition to the dynamic monthly trends observed in LO-OOA, there are also strong spatial variabilities for these two key ions (i.e., m/z 44 and m/z 43). The IQR/median ratios of f_{44} and f_{43} in LO-OOA are in the range 0.38–0.94 and 0.39–0.60, respectively. This is expected considering LO-OOA has never been constrained, and various ageing processes, precursors, and meteorological conditions could contribute to the large spatial variabilities. When we sum up the LO-OOA and MO-OOA to the Total OOA factor, m/z 44 is still the dominating ion with an average of 0.21, but it is smaller than that of MO-OOA alone due to the much smaller f_{44} in LO-OOA with an average of 0.14. Overall, f_{43} in the Total OOA factor still shows an increasing trend during warm seasons like the LO-OOA factor, which indicates that the effect of enhanced biogenic emissions on the intensity of f_{43} in the Total OOA might be rather considerable. Moreover, f_{43} in the Total OOA shows relatively

smaller spatial variabilities (compared to MO-OOA and LO-OOA) with an IQR/median ratio of 0.26–0.41. The f_{44} in the Total OOA has slightly larger spatial variabilities than MO-OOA with an IQR/median ratio of 0.21–0.40, but it is still more stable than LO-OOA. It is expected considering the large spatial variabilities in LO-OOA. However, the sum of the OOA factors shows little monthly trends except for the increasing f_{43} (thus, decreasing f_{44}) in warmer months (May-September).

4. Conclusion

A state-of-the-art standardised protocol for source apportionment of long-term ACSM/AMS organic aerosol mass spectrum datasets was developed. Our protocol was validated systematically and strictly applied to 22 sites with year-long measurements. It demonstrates the consistency of this protocol with comprehensive source apportionment results, even though each dataset was analysed by each research group individually. Our source apportionment strategy has been significantly improved compared to conventional seasonal PMF by utilising rolling windows, bootstrap, and ME-2 techniques, which were first introduced by Canonaco et al. (2021). As addressed by Chen et al. (2021) and Tobler et al. (2021), this strategy allows us to retrieve robust source apportionment results by considering temporal variations of source profiles. Importantly, the success of the rolling mechanism is an essential step to make real-time source apportionment possible (Chen et al., 2022). However, the current protocol/strategy remains challenging to objectively define the transition point to an improved source apportionment for rolling PMF analysis when a different number of OA factors is necessary for different periods. More tools should be tested to address this challenge in the near future.

Overall, this work provides a comprehensive overview of the OA sources in Europe with highly time-resolved source apportionment results. The OA fraction in PM$_1$ is high (23–75%) across Europe and seasons. With the help of this advanced source apportionment strategy, many common POA factors have been resolved, including HOA, COA, BBOA, CCOA, and SFOA, together with secondary OOA factors, i.e., MO-OOA and LO-OOA in these 22 datasets. Moreover, some local OA components have been identified at specific stations, like a coffee roastery OA factor in Helsinki, a ship industry OA factor in Marseille, a sea salt factor in Carnsore Point, and a cigarette smoke OA factor in Zürich. The OOA factors together constitute the main contributor (47.3–100%) to OA and generally show more stable diel and weekly cycles than POA factors. The contributions of POA increase with increasing total OA mass concentration in most of the polluted regions. It suggests that the control of primary emissions could help mitigate OA mass concentration or at least decrease the likelihood of highly polluted episodes. Also, most POA factors show enhanced contribution/mass concentrations during cold seasons compared to warm seasons due to residential heating. Lower boundary layer heights (lower temperature) combined with stagnant

Table 2
Normalised spatial variations for key ions using the interquartile range (IQR) divided by the medians of average monthly intensities across the 22 datasets.

Factors	HOA		COA		BBOA		MO-OOA		LO-OOA		Total OOA	
m/z	55	57	55	57	60	73	44	43	44	43	44	43
Jan	0.13	0.21	0.11	0.04	0.36	0.29	0.30	0.46	0.52	0.46	0.34	0.34
Feb	0.16	0.19	0.12	0.04	0.33	0.35	0.25	0.57	0.60	0.54	0.31	0.29
Mar	0.15	0.19	0.10	0.11	0.37	0.25	0.28	0.45	0.57	0.39	0.26	0.39
Apr	0.12	0.22	0.06	0.10	0.36	0.25	0.27	0.69	0.60	0.60	0.32	0.39
May	0.17	0.24	0.09	0.11	0.36	0.23	0.34	0.83	0.86	0.53	0.37	0.36
Jun	0.19	0.17	0.11	0.17	0.34	0.20	0.27	0.81	0.63	0.53	0.40	0.33
Jul	0.19	0.21	0.18	0.17	0.32	0.21	0.27	0.65	0.38	0.40	0.29	0.29
Aug	0.21	0.27	0.27	0.14	0.28	0.22	0.26	0.69	0.50	0.43	0.29	0.30
Sep	0.19	0.21	0.24	0.04	0.32	0.23	0.25	0.70	0.94	0.41	0.36	0.33
Oct	0.11	0.18	0.25	0.06	0.39	0.21	0.27	0.49	0.46	0.59	0.30	0.26
Nov	0.11	0.13	0.19	0.08	0.34	0.36	0.19	0.60	0.50	0.55	0.21	0.41
Dec	0.12	0.22	0.14	0.02	0.33	0.36	0.16	0.77	0.74	0.42	0.29	0.39
Mean	0.15 ± 0.03	0.20 ± 0.03	0.16 ± 0.07	0.09 ± 0.05	0.34 ± 0.03	0.26 ± 0.06	0.26 ± 0.05	0.64 ± 0.13	0.61 ± 0.16	0.49 ± 0.08	0.40 ± 0.05	0.34 ± 0.05

conditions can readily cause the accumulation of pollutants. In particular, HOA (traffic emissions) is a non-negligible OA source with a rather consistent contribution across different stations (10.7 ± 3.8%). Six urban sites display a significant COA factor (i.e., two Athens datasets, Zürich, London, Barcelona, and Marseille) with an overall average contribution to OA of 14.5 ± 2.5%. Moreover, most of the datasets show a resolved BBOA component (except Hyytiälä, Puy de Dôme, and Helsinki) with important contributions to OA (annual average:12.4 ± 6.9%), which increases substantially in winter, with a contribution of 16.9 ± 8.4%. Melpitz and Kraków present a CCOA factor (annual average: 14.7 ± 0.8%, winter average: 20.6 ± 3.5%), while SFOA is found to be heavily affected by peat and coal combustion sources at Carnsore Point and Dublin (annual average: 19.3 ± 10.4%, winter average: 22.7 ± 14.4%). All of these results confirm that the reduction of solid fuel-burning for residential heating is one of the key leverages to mitigate fine PM levels in Europe, especially in winter.

This study reveals the spatial and seasonal concentration variability of the MO-OOA, LO-OOA, and Total OOA factors. MO-OOA and Total OOA show little variability, while LO-OOA varies considerably across spatial and seasonal domains. This is expected since the ageing processes, abundances/types of precursors and meteorological conditions can differ both temporally and spatially. In particular, the seasonality of the LO-OOA factor in most of the datasets agrees well with the findings reported by Canonaco et al. 2015), with increasing f_{43} (thus, decreasing f_{44}) intensity in warm seasons likely due to the enhanced biogenic emissions.

Moreover, with the help of the rolling PMF technique, time-dependent OA factor profiles have been retrieved. Therefore, this study also investigates the monthly trends (averaged over 22 datasets) and corresponding variabilities (IQR/median ratio) across sites for key ions in the commonly resolved OA factors. While these key ions barely show monthly trends in HOA, COA, MO-OOA, and Total OOA, BBOA key ion (f_{60} and f_{73}) intensities increase during the cold seasons due to the abundance of biomass burning sources and the lower reactivity of levoglucosan. The increased f_{43} of LO-OOA during warm seasons is most likely due to enhanced biogenic SOA formation. In terms of spatial variabilities, key ions for HOA and COA factors show a small IQR/median ratio with a range of 0.06–0.27 due to both factor contributions being consistent (if present), as reported in previous studies. However, the key ions for the BBOA factor show a relatively larger spatial variability with the IQR/median ratio ranging from 0.20 to 0.39, which suggests potentially different combustion conditions, type of woods, etc., contribute to this variability in the real-world scenarios. In addition, the f_{43} intensities in MO-OOA and LO-OOA show large spatial variability, with the IQR/median ratio ranging from 0.45 to 0.83 and 0.39 to 0.60, respectively. The f_{44} in LO-OOA has a large IQR/median ratio range of 0.38–0.94, but the f_{44} in MO-OOA is rather less variable across sites with a relatively small IQR/median ratio range of 0.16–0.34. This is expected, since OOA factors are never constrained combined and complex ageing processes are affected by different locations and meteorological conditions. OOA is the dominant contributor to OA, but ACSM data alone is insufficient for its apportionment to specific sources and formation mechanisms. Back-trajectory analysis could support the understanding of the source regions and transportation pathways for long-range transported OOA. Model – measurement assessments may be used to further constrain the secondary organic aerosol formation sources and pathways. In addition, higher m/z resolving ability and time resolution instrumentation (e.g., FIGAERO (Lopez-Hilfiker et al., 2014), EESI-TOF (Lopez-Hilfiker et al., 2019), and EESI-Orbitrap (Lee et al., 2020)) could provide more information at the molecular level of OA, which can help us to separate OOA factors better when conducting PMF (Qi et al., 2019; Stefenelli et al., 2019). Such instruments are not yet developed for long-term use, but they could be used in campaigns or for filter analyses that are taken concurrently with the on-line data. Moreover, offline-AMS (Daellenbach et al., 2016) analyses could be useful to better explain seasonal variabilities of the dominant contributors of

OOA. With the help of this state-of-the-art source apportionment protocol, this study has retrieved highly time-resolved, long-term (>9 months), and robust OA source information consistently, with minimum subjective judgements. This highly time-resolved comprehensive OA source information can be useful inputs/constraints to improve/validate climate, health, and air quality models.

Finally, this work suggests that policymakers should address the major combustion sources (i.e., biomass burning, coal combustion, and peat) that affect air quality in Europe. Besides, more attention should be paid to the traffic source, even though it is quite constant across places because it is significant in organic aerosols and is also a proxy for non-exhaust emissions. Due to regional transport, decreasing the emissions of primary factors would also decrease the secondary factors observed at the non-urban sites.

CRediT authorship contribution statement

Gang Chen: Conceptualization, Data curation, Formal analysis, Investigation, Methodology, Project administration, Software, Validation, Visualization, Writing – original draft, Writing – review & editing. **Francesco Canonaco:** Methodology, Software, Writing – review & editing. **Anna Tobler:** Data curation, Formal analysis, Investigation, Software, Visualization, Writing – review & editing. **Wenche Aas:** Data curation, Funding acquisition, Supervision. **Andres Alastuey:** Data curation, Funding acquisition, Supervision. **James Allan:** Investigation. **Samira Atabakhsh:** Data curation, Formal analysis, Investigation. **Minna Aurela:** Data curation, Formal analysis, Investigation, Writing – review & editing. **Urs Baltensperger:** Supervision, Validation, Writing – review & editing. **Aikaterini Bougiatioti:** Data curation, Formal analysis, Investigation. **Joel F. De Brito:** Formal analysis, Investigation. **Darius Ceburnis:** Funding acquisition, Supervision. **Benjamin Chazeau:** Data curation, Formal analysis, Investigation, Software. **Hasna Chebaicheb:** Data curation, Formal analysis, Investigation. **Kaspar R. Daellenbach:** Investigation. **Mikael Ehn:** Funding acquisition, Supervision. **Imad El Haddad:** . **Konstantinos Eleftheriadis:** Formal analysis, Funding acquisition, Investigation, Supervision. **Olivier Favez:** Funding acquisition, Supervision. **Harald Flentje:** Data curation. **Anna Font:** Data curation, Formal analysis, Investigation, Writing – review & editing. **Kirsten Fossum:** Data curation, Formal analysis. **Evelyn Freney:** Data curation, Formal analysis, Investigation, Writing – review & editing. **Maria Gini:** Data curation, Formal analysis, Investigation. **David C Green:** Data curation, Funding acquisition, Investigation, Supervision. **Liine Heikkinen:** Data curation, Formal analysis, Investigation, Writing – review & editing. **Hartmut Herrmann:** Funding acquisition, Investigation, Supervision. **Athina-Cerise Kalogridis:** Resources. **Hannes Keernik:** Data curation, Formal analysis, Investigation. **Radek Lhotka:** Data curation, Formal analysis, Investigation. **Chunshui Lin:** Data curation, Formal analysis. **Chris Lunder:** Data curation, Investigation. **Marek Maasikmets:** Funding acquisition. **Manousos I. Manousakas:** Data curation. **Nicolas Marchand:** Formal analysis, Funding acquisition, Investigation, Writing – review & editing. **Cristina Marin:** Data curation. **Luminita Marmureanu:** Data curation. **Nikolaos Mihalopoulos:** Formal analysis, Funding acquisition, Investigation, Supervision. **Griša Močnik:** Investigation, Resources. **Jaroslaw Nęcki:** Resources. **Colin O'Dowd:** Funding acquisition, Supervision. **Jurgita Ovadnevaite:** Data curation, Funding acquisition, Investigation, Supervision. **Thomas Peter:** Supervision. **Jean-Eudes Petit:** Data curation, Formal analysis, Investigation, Supervision. **Michael Pikridas:** Data curation, Formal analysis. **Stephen Matthew Platt:** Formal analysis, Writing – review & editing, Investigation. **Petra Pokorná:** Data curation, Funding acquisition, Investigation, Supervision. **Laurent Poulain:** Data curation, Formal analysis, Funding acquisition, Investigation, Supervision. **Max Priestman:** Data curation, Investigation. **Véronique Riffault:** Data curation, Formal analysis, Funding acquisition, Investigation, Supervision, Writing – review & editing. **Matteo Rinaldi:** Funding acquisition, Supervision. **Kazimierz Różański:**

Supervision. **Jaroslav Schwarz:** Formal analysis, Funding acquisition. **Jean Sciare:** Funding acquisition, Writing – review & editing. **Leïla Simon:** Data curation, Formal analysis, Investigation, Supervision. **Alicja Skiba:** Investigation. **Jay G. Slowik:** Funding acquisition, Investigation, Methodology, Software, Writing – review & editing. **Yulia Sosedova:** Formal analysis, Data curation. **Iasonas Stavroulas:** Data curation, Funding acquisition, Investigation, Supervision. **Katarzyna Styszko:** Investigation, Resources. **Erik Teinemaa:** Funding acquisition. **Hilkka Timonen:** Funding acquisition. **Anja Tremper:** Writing – review & editing. **Jeni Vasilescu:** Formal analysis, Funding acquisition, Investigation, Writing – review & editing. **Marta Via:** Data curation, Formal analysis, Investigation. **Petr Vodička:** Data curation, Investigation. **Alfred Wiedensohler:** Funding acquisition, Investigation, Supervision. **Olga Zografou:** Data curation, Formal analysis, Investigation. **María Cruz Minguillón:** Conceptualization, Funding acquisition, Investigation, Project administration, Resources. **André S. H. Prévôt:** Conceptualization, Funding acquisition, Investigation, Supervision, Methodology, Project administration, Resources, Validation, Writing – review & editing.

Declaration of Competing Interest

The authors declare that they have no known competing financial interests or personal relationships that could have appeared to influence the work reported in this paper.

Data availability

The time series of resolved source apportionment results and corresponding external data as well as detailed description of rolling PMF settings are publicly available (DOI: [10.5281/zenodo.6522811](https://doi.org/10.5281/zenodo.6522811)).

Appendix A. Supplementary material

Supplementary data to this article can be found online at https://doi.org/10.1016/j.envint.2022.107325.

References

Äijälä, M., Heikkinen, L., Fröhlich, R., Canonaco, F., Prévôt, A.S.H., Junninen, H., Petäjä, T., Kulmala, M., Worsnop, D., Ehn, M., 2017. Resolving anthropogenic aerosol pollution types – deconvolution and exploratory classification of pollution events. Atmos. Chem. Phys. 17, 3165–3197. https://doi.org/10.5194/acp-17-3165-2017.

Barreira, L.M.F., Ylisirniö, A., Pullinen, I., Buchholz, A., Li, Z., Lipp, H., Junninen, H., Hõrrak, U., Noe, S.M., Krasnova, A., Krasnov, D., Kask, K., Talts, E., Niinemets, Ü., Ruiz-Jimenez, J., Schobesberger, S., 2021. The importance of sesquiterpene oxidation products for secondary organic aerosol formation in a springtime hemiboreal forest. Atmos. Chem. Phys. 21, 11781–11800. https://doi.org/10.5194/acp-21-11781-2021.

Bertrand, A., Stefenelli, G., Jen, C.N., Pieber, S.M., Bruns, E.A., Ni, H., Temime-Roussel, B., Slowik, J.G., Goldstein, A.H., El Haddad, I., Baltensperger, U., Prévôt, A. S.H., Wortham, H., Marchand, N., 2018. Evolution of the chemical fingerprint of biomass burning organic aerosol during aging. Atmos. Chem. Phys. 18, 7607–7624. https://doi.org/10.5194/acp-18-7607-2018.

Bougiatioti, A., Stavroulas, I., Kostenidou, E., Zarmpas, P., Theodosi, C., Kouvarakis, G., Canonaco, F., Prévôt, A.S.H., Nenes, A., Pandis, S.N., Mihalopoulos, N., 2014. Processing of biomass-burning aerosol in the eastern Mediterranean during summertime. Atmos. Chem. Phys. 14, 4793–4807. https://doi.org/10.5194/acp-14-4793-2014.

Bressi, M., Cavalli, F., Putaud, J.P., Fröhlich, R., Petit, J.-E., Aas, W., Äijälä, M., Alastuey, A., Allan, J.D., Aurela, M., Berico, M., Bougiatioti, A., Bukowiecki, N., Canonaco, F., Crenn, V., Dusanter, S., Ehn, M., Elsasser, M., Flentje, H., Graf, P., Green, D.C., Heikkinen, L., Hermann, H., Holzinger, R., Hueglin, C., Keernik, H., Kiendler-Scharr, A., Kubelová, L., Lunder, C., Maasikmets, M., Makeš, O., Malaguti, A., Mihalopoulos, N., Nicolas, J.B., O'Dowd, C., Ovadnevaite, J., Petralia, E., Poulain, L., Priestman, M., Riffault, V., Ripoll, A., Schlag, P., Schwarz, J., Sciare, J., Slowik, J., Sosedova, Y., Stavroulas, I., Teinemaa, E., Via, M., Vodička, P., Williams, P.I., Wiedensohler, A., Young, D.E., Zhang, S., Favez, O., Minguillón, M.C., Prevot, A.S.H., 2021. A European aerosol phenomenology - 7: High-time resolution chemical characteristics of submicron particulate matter across Europe. Atmos. Environ. X 10, 100108. https://doi.org/10.1016/j.aeaoa.2021.100108.

Canonaco, F., Crippa, M., Slowik, J.G., Baltensperger, U., Prévôt, A.S.H., 2013. SoFi, an IGOR-based interface for the efficient use of the generalized multilinear engine (ME-2) for the source apportionment: ME-2 application to aerosol mass spectrometer data. Atmos. Meas. Tech. 6, 3649–3661. https://doi.org/10.5194/amt-6-3649-2013.

Canonaco, F., Slowik, J.G., Baltensperger, U., Prévôt, A.S.H., 2015. Seasonal differences in oxygenated organic aerosol composition: implications for emissions sources and factor analysis. Atmos. Chem. Phys. 15, 6993–7002. https://doi.org/10.5194/acp-15-6993-2015.

Canonaco, F., Tobler, A., Chen, G., Sosedova, Y., Slowik, J.G., Bozzetti, C., Daellenbach, K.R., El Haddad, I., Crippa, M., Huang, R.-J., Furger, M., Baltensperger, U., Prévôt, A.S.H., 2021. A new method for long-term source apportionment with time-dependent factor profiles and uncertainty assessment using SoFi Pro: application to 1 year of organic aerosol data. Atmos. Meas. Tech. 14, 923–943. https://doi.org/10.5194/amt-14-923-2021.

Casotto, R., Skiba, A., Rauber, M., Strähl, J., Tobler, A., Bhattu, D., Lamkaddam, H., Manousakas, M.I., Salazar, G., Ryś, A., Haddad, I.E., Kasper-Giebl, A., Baltensperger, U., Necki, J., Szidat, S., Styszko, K., Slowik, J.G., Daellenbach, K.R., 2022. Organic aerosol sources in Krakow, Poland, before implementation of a solid fuel residential heating ban. Sci. Total Environ. (submitted for publication).

Chazeau, B., El Haddad, I., Canonaco, F., Temime-Roussel, B., D'Anna, B., Gille, G., Mesbah, B., Prévôt, A.S.H., Wortham, H., Marchand, N., 2022. Organic aerosol source apportionment by using rolling positive matrix factorization: application to a Mediterranean coastal city. Atmospheric Environ.: X 14, 100176. https://doi.org/10.1016/j.aeaoa.2022.100176.

Chazeau, B., Temime-Roussel, B., Gille, G., Mesbah, B., D'Anna, B., Wortham, H., Marchand, N., 2021. Measurement report: fourteen months of real-time characterisation of the submicronic aerosol and its atmospheric dynamics at the Marseille-Longchamp supersite. Atmos. Chem. Phys. 21, 7293–7319. https://doi.org/10.5194/acp-21-7293-2021.

Chen, G., Canonaco, F., Slowik, J.G., Dallenbach, K.R., Tobler, A.K., Petit, J., Favez, O., Stavroulas, I., Mihalopoulos, N., Gerasopoulos, E., Baltensperger, U., Prévôt, A.S.H., 2022. Real-time source apportionment of organic aerosols in three european cities. Environmental Science & Technology. Submitted for publication.

Chen, G., Sosedova, Y., Canonaco, F., Fröhlich, R., Tobler, A., Vlachou, A., Daellenbach, K.R., Bozzetti, C., Hueglin, C., Graf, P., Baltensperger, U., Slowik, J.G., El Haddad, I., Prévôt, A.S.H., 2021. Time-dependent source apportionment of submicron organic aerosol for a rural site in an alpine valley using a rolling positive matrix factorisation (PMF) window. Atmospheric Chem. Phys. https://doi.org/10.5194/acp-21-15081-2021.

COLOSSAL, 2021. Guidelines for comparison of ACSM measurements with co-located external data [WWW Document]. URL http://www.actris-ecac.eu/pmc-non-refractory-organics-and-inorganics.html%0A (accessed 12.20.21).

Crenn, V., Sciare, J., Croteau, P.L., Verlhac, S., Fröhlich, R., Belis, C.A., Aas, W., Äijälä, M., Alastuey, A., Artíñano, B., Baisnée, D., Bonnaire, N., Bressi, M., Canagaratna, M., Canonaco, F., Carbone, C., Cavalli, F., Coz, E., Cubison, M.J., Esser-Gietl, J.K., Green, D.C., Gros, V., Heikkinen, L., Herrmann, H., Lunder, C., Minguillón, M.C., Močnik, G., O'Dowd, C.D., Ovadnevaite, J., Petit, J.-E., Petralia, E., Poulain, L., Priestman, M., Riffault, V., Ripoll, A., Sarda-Estève, R., Slowik, J.G., Setyan, A., Wiedensohler, A., Baltensperger, U., Prévôt, A.S.H., Jayne, J.T., Favez, O., 2015. ACTRIS ACSM intercomparison – Part 1: Reproducibility of concentration and fragment results from 13 individual Quadrupole Aerosol Chemical Speciation Monitors (Q-ACSM) and consistency with co-located instruments. Atmos. Meas. Tech. 8, 5063–5087. https://doi.org/10.5194/amt-8-5063-2015.

Crippa, M., Canonaco, F., Lanz, V.A., Äijälä, M., Allan, J.D., Carbone, S., Capes, G., Ceburnis, D., Dall'Osto, M., Day, D.A., DeCarlo, P.F., Ehn, M., Eriksson, A., Freney, E., Hildebrandt Ruiz, L., Hillamo, R., Jimenez, J.L., Junninen, H., Kiendler-Scharr, A., Kortelainen, A.-M., Kulmala, M., Laaksonen, A., Mensah, A.A., Mohr, C.,

Nemitz, E., O'Dowd, C., Ovadnevaite, J., Pandis, S.N., Petäjä, T., Poulain, L., Saarikoski, S., Sellegri, K., Swietlicki, E., Tiitta, P., Worsnop, D.R., Baltensperger, U., Prévôt, A.S.H., 2014. Organic aerosol components derived from 25 AMS data sets across Europe using a consistent ME-2 based source apportionment approach. Atmos. Chem. Phys. 14 (12), 6159–6176. https://doi.org/10.5194/acp-14-6159-2014.

Crippa, M., DeCarlo, P.F., Slowik, J.G., Mohr, C., Heringa, M.F., Chirico, R., Poulain, L., Freutel, F., Sciare, J., Cozic, J., Di Marco, C.F., Elsasser, M., Nicolas, J.B., Marchand, N., Abidi, E., Wiedensohler, A., Drewnick, F., Schneider, J., Borrmann, S., Nemitz, E., Zimmermann, R., Jaffrezo, J.-L., Prévôt, A.S.H., Baltensperger, U., 2013. Wintertime aerosol chemical composition and source apportionment of the organic fraction in the metropolitan area of Paris. Atmos. Chem. Phys. 13, 961–981. https://doi.org/10.5194/acp-13-961-2013.

Cubison, M.J., Ortega, A.M., Hayes, P.L., Farmer, D.K., Day, D., Lechner, M.J., Brune, W. H., Apel, E., Diskin, G.S., Fisher, J.A., Fuelberg, H.E., Hecobian, A., Knapp, D.J., Mikoviny, T., Riemer, D., Sachse, G.W., Sessions, W., Weber, R.J., Weinheimer, A.J., Wisthaler, A., Jimenez, J.L., 2011. Effects of aging on organic aerosol from open biomass burning smoke in aircraft and laboratory studies. Atmos. Chem. Phys. 11 (23), 12049–12064. https://doi.org/10.5194/acp-11-12049-2011.

Daellenbach, K.R., Bozzetti, C., Křepelová, A., Canonaco, F., Wolf, R., Zotter, P., Fermo, P., Crippa, M., Slowik, J.G., Sosedova, Y., Zhang, Y., Huang, R.-J.-J., Poulain, L., Szidat, S., Baltensperger, U., El Haddad, I., Prévôt, A.S.H., 2016. Characterization and source apportionment of organic aerosol using offline aerosol mass spectrometry. Atmos. Meas. Tech. 9, 23–39. https://doi.org/10.5194/amt-9-23-2016.

Daellenbach, K.R., Uzu, G., Jiang, J., Cassagnes, L.-E., Leni, Z., Vlachou, A., Stefenelli, G., Canonaco, F., Weber, S., Segers, A., Kuenen, J.J.P., Schaap, M., Favez, O., Albinet, A., Aksoyoglu, S., Dommen, J., Baltensperger, U., Geiser, M., El Haddad, I., Jaffrezo, J.-L., Prévôt, A.S.H., 2020. Sources of particulate-matter air pollution and its oxidative potential in Europe. Nature 587, 414–419. https://doi.org/10.1038/s41586-020-2902-8.

Drewnick, F., Hings, S.S., DeCarlo, P., Jayne, J.T., Gonin, M., Fuhrer, K., Weimer, S., Jimenez, J.L., Demerjian, K.L., Borrmann, S., Worsnop, D.R., 2005. A new time-of-flight aerosol mass spectrometer (TOF-AMS)—instrument description and first field deployment. Aerosol Sci. Technol. 39, 637–658. https://doi.org/10.1080/02786820500182040.

Efron, B., 1979. Bootstrap methods: another look at the jackknife. Ann. Stat. 7, 1–26.

Elser, M., Bozzetti, C., El-Haddad, I., Maasikmets, M., Teinemaa, E., Richter, R., Wolf, R., Slowik, J.G., Baltensperger, U., Prévôt, A.S.H., 2016. Urban increments of gaseous and aerosol pollutants and their sources using mobile aerosol mass spectrometry measurements. Atmos. Chem. Phys. Discuss. 2016, 7117–7134. https://doi.org/10.5194/acp-2016-31.

European Environment Agency (EEA), 2021. Air quality in Europe 2021. Copenhagen, Denmark. 10.2800/549289.

Farah, A., Freney, E., Canonaco, F., Prévôt, A.S.H., Pichon, J., Abboud, M., Farah, W., Sellegri, K., 2021. Altitude aerosol measurements in central france: seasonality, sources and free-troposphere/boundary layer segregation. Earth Sp. Sci. 8 https://doi.org/10.1029/2019EA001018.

Freney, E., Zhang, Y., Croteau, P., Amodeo, T., Williams, L., Truong, F., Petit, J.E., Sciare, J., Sarda-Esteve, R., Bonnaire, N., Arumae, T., Aurela, M., Bougiatioti, A., Mihalopoulos, N., Coz, E., Artinano, B., Crenn, V., Elste, T., Heikkinen, L., Poulain, L., Wiedensohler, A., Herrmann, H., Priestman, M., Alastuey, A., Stavroulas, I., Tobler, A., Vasilescu, J., Zanca, N., Canagaratna, M., Carbone, C., Flentje, H., Green, D., Maasikmets, M., Marmureanu, L., Minguillon, M.C., Prevot, A. S.H., Gros, V., Jayne, J., Favez, O., 2019. The second ACTRIS inter-comparison (2016) for Aerosol Chemical Speciation Monitors (ACSM): Calibration protocols and instrument performance evaluations. Aerosol Sci. Technol. 53, 830–842. https://doi.org/10.1080/02786826.2019.1608901.

Fröhlich, R., Crenn, V., Setyan, A., Belis, C.A., Canonaco, F., Favez, O., Riffault, V., Slowik, J.G., Aas, W., Äijälä, M., Alastuey, A., Artiñano, B., Bonnaire, N., Bozzetti, C., Bressi, M., Carbone, C., Coz, E., Croteau, P.L., Cubison, M.J., Esser-Gietl, J.K., Green, D.C., Gros, V., Heikkinen, L., Herrmann, H., Jayne, J.T., Lunder, C.R., Minguillón, M.C., Močnik, G., O'Dowd, C.D., Ovadnevaite, J., Petralia, E., Poulain, L., Priestman, M., Ripoll, A., Sarda-Estève, R., Wiedensohler, A., Baltensperger, U., Sciare, J., Prévôt, A.S.H., 2015. ACTRIS ACSM intercomparison – Part 2: Intercomparison of ME-2 organic source apportionment results from 15 individual, co-located aerosol mass spectrometers. Atmos. Meas. Tech. 8, 2555–2576. https://doi.org/10.5194/amt-8-2555-2015.

Fröhlich, R., Cubison, M.J., Slowik, J.G., Bukowiecki, N., Prévôt, A.S.H., Baltensperger, U., Schneider, J., Kimmel, J.R., Gonin, M., Rohner, U., Worsnop, D.R., Jayne, J.T., 2013. The ToF-ACSM: a portable aerosol chemical speciation monitor with TOFMS detection. Atmos. Meas. Tech. 6, 3225–3241. https://doi.org/10.5194/amt-6-3225-2013.

Fuller, G.W., Tremper, A.H., Baker, T.D., Yttri, K.E., Butterfield, D., 2014. Contribution of wood burning to PM10 in London. Atmos. Environ. 87, 87–94. https://doi.org/10.1016/j.atmosenv.2013.12.037.

Grieshop, A.P., Donahue, N.M., Robinson, A.L., 2009. Laboratory investigation of photochemical oxidation of organic aerosol from wood fires 2: analysis of aerosol mass spectrometer data. Atmos. Chem. Phys. 9, 2227–2240. https://doi.org/10.5194/acp-9-2227-2009.

Heikkinen, L., Äijälä, M., Daellenbach, K.R., Chen, G., Garmash, O., Aliaga, D., Graeffe, F., Räty, M., Luoma, K., Aalto, P., Kulmala, M., Petäjä, T., Worsnop, D., Ehn, M., 2021. Eight years of sub-micrometre organic aerosol composition data from the boreal forest characterized using a machine-learning approach. Atmos. Chem. Phys. 21, 10081–10109. https://doi.org/10.5194/acp-21-10081-2021.

Heringa, M.F., DeCarlo, P.F., Chirico, R., Tritscher, T., Dommen, J., Weingartner, E., Richter, R., Wehrle, G., Prévôt, A.S.H., Baltensperger, U., 2011. Investigations of primary and secondary particulate matter of different wood combustion appliances with a high-resolution time-of-flight aerosol mass spectrometer. Atmos. Chem. Phys. 11, 5945–5957. https://doi.org/10.5194/acp-11-5945-2011.

Hinds, W.C., 1999. Aerosol Technology: Properties, Behavior, and Measurement of Airborne Particles, 2nd Edition, 2nd ed. A WILEY -INTERSCIENCE PUBLICATION. John Wiley & SONS, INC., NEW YORK/CHICHESTER/WEINHEIM/BRISBANE/ SINGAPORE/TORONTO.

IPCC, 2021. AR6 Climate Change 2021: The Physical Science Basis. Cambridge University Press.

Jayne, J.T., Leard, D.C., Zhang, X., Davidovits, P., Smith, K.A., Kolb, C.E., Worsnop, D.R., 2000. Development of an aerosol mass spectrometer for size and composition analysis of submicron particles. Aerosol Sci. Technol. 33, 49–70. https://doi.org/10.1080/027868200410840.

Jimenez, J.L., Canagaratna, M.R., Donahue, N.M., Prevot, A.S.H., Zhang, Q., Kroll, J.H., DeCarlo, P.F., Allan, J.D., Coe, H., Ng, N.L., Aiken, A.C., Docherty, K.S., Ulbrich, I.M., Grieshop, A.P., Robinson, A.L., Duplissy, J., Smith, J.D., Wilson, K.R., Lanz, V.A., Hueglin, C., Sun, Y.L., Tian, J., Laaksonen, A., Raatikainen, T., Rautiainen, J., Vaattovaara, P., Ehn, M., Kulmala, M., Tomlinson, J.M., Collins, D.R., Cubison, M.J., Dunlea, J., Huffman, J.A., Onasch, T.B., Alfarra, M.R., Williams, P.I., Bower, K., Kondo, Y., Schneider, J., Drewnick, F., Borrmann, S., Weimer, S., Demerjian, K., Salcedo, D., Cottrell, L., Griffin, R., Takami, A., Miyoshi, T., Hatakeyama, S., Shimono, A., Sun, J.Y., Zhang, Y.M., Dzepina, K., Kimmel, J.R., Sueper, D., Jayne, J.T., Herndon, S.C., Trimborn, A.M., Williams, L.R., Wood, E.C., Middlebrook, A.M., Kolb, C.E., Baltensperger, U., Worsnop, D.R., 2009. Evolution of organic aerosols in the atmosphere. Science (80-.) 326 (5959), 1525–1529. https://doi.org/10.1126/science.1180353.

Kodros, J.K., Papanastasiou, D.K., Paglione, M., Masiol, M., Squizzato, S., Florou, K., Skyllakou, K., Kaltsonoudis, C., Nenes, A., Pandis, S.N., 2020. Rapid dark aging of biomass burning as an overlooked source of oxidized organic aerosol. Proc. Natl. Acad. Sci. 117, 33028–33033. https://doi.org/10.1073/pnas.2010365117.

Lanz, V.A., Alfarra, M.R., Baltensperger, U., Buchmann, B., Hueglin, C., Prévôt, A.S.H., 2007. Source apportionment of submicron organic aerosols at an urban site by factor analytical modelling of aerosol mass spectra. Atmos. Chem. Phys. 7, 1503–1522. https://doi.org/10.5194/acp-7-1503-2007.

Lanz, V.A., Prévôt, A.S.H., Alfarra, M.R., Weimer, S., Mohr, C., DeCarlo, P.F., Gianini, M.F.D., Hueglin, C., Schneider, J., Favez, O., D'Anna, B., George, C., Baltensperger, U., 2010. Characterization of aerosol chemical composition with aerosol mass spectrometry in Central Europe: an overview. Atmos. Chem. Phys. 10 (21), 10453–10471. https://doi.org/10.5194/acp-10-10453-2010.

Lee, C.P., Riva, M., Wang, D., Tomaz, S., Li, D., Perrier, S., Slowik, J.G., Bourgain, F., Schmale, J., Prevot, A.S.H., Baltensperger, U., George, C., El Haddad, I., 2020. Online chemical characterization by extractive electrospray ionization–ultrahigh-resolution mass spectrometry (EESI-Orbitrap). Environ. Sci. Technol. 54, 3871–3880. https://doi.org/10.1021/acs.est.9b07090.

Lin, C., Ceburnis, D., Huang, R.-J., Xu, W., Spohn, T., Martin, D., Buckley, P., Wenger, J., Hellebust, S., Rinaldi, M., Facchini, M.C., O'Dowd, C., Ovadnevaite, J., 2019. Wintertime aerosol dominated by solid-fuel-burning emissions across Ireland: insight into the spatial and chemical variation in submicron aerosol. Atmos. Chem. Phys. 19, 14091–14106. https://doi.org/10.5194/acp-19-14091-2019.

Lin, C., Huang, R.-J., Ceburnis, D., Buckley, P., Preissler, J., Wenger, J., Rinaldi, M., Facchini, M.C., O'Dowd, C., Ovadnevaite, J., 2018. Extreme air pollution from residential solid fuel burning. Nat. Sustain. 1, 512–517. https://doi.org/10.1038/s41893-018-0125-x.

Liu, C., Chen, R., Sera, F., Vicedo-Cabrera, A.M., Guo, Y., Tong, S., Coelho, M.S.Z.S., Saldiva, P.H.N., Lavigne, E., Matus, P., Valdes Ortega, N., Osorio Garcia, S., Pascal, M., Stafoggia, M., Scortichini, M., Hashizume, M., Honda, Y., Hurtado-Díaz, M., Cruz, J., Nunes, B., Teixeira, J.P., Kim, H., Tobias, A., Íñiguez, C., Forsberg, B., Åström, C., Ragettli, M.S., Guo, Y.-L., Chen, B.-Y., Bell, M.L., Wright, C.Y., Scovronick, N., Garland, R.M., Milojevic, A., Kyselý, J., Urban, A., Orru, H., Indermitte, E., Jaakkola, J.J.K., Ryti, N.R.I., Katsouyanni, K., Analitis, A., Zanobetti, A., Schwartz, J., Chen, J., Wu, T., Cohen, A., Gasparrini, A., Kan, H., 2019. Ambient particulate air pollution and daily mortality in 652 cities. N. Engl. J. Med. 381, 705–715. https://doi.org/10.1056/NEJMoa1817364.

Lopez-Hilfiker, F.D., Mohr, C., Ehn, M., Rubach, F., Kleist, E., Wildt, J., Mentel, T.F., Lutz, A., Hallquist, M., Worsnop, D., Thornton, J.A., 2014. A novel method for online analysis of gas and particle composition: description and evaluation of a Filter Inlet for Gases and AEROsols (FIGAERO). Atmos. Meas. Tech. 7, 983–1001. https://doi.org/10.5194/amt-7-983-2014.

Lopez-Hilfiker, F.D., Pospisilova, V., Huang, W., Kalberer, M., Mohr, C., Stefenelli, G., Thornton, J.A., Baltensperger, U., Prevot, A.S.H., Slowik, J.G., 2019. An Extractive Electrospray Ionization Time-of-Flight Mass Spectrometer (EESI-TOF) for online measurement of atmospheric aerosol particles. Atmos. Meas. Tech. 12, 4867–4886. https://doi.org/10.5194/amt-12-4867-2019.

Minguillón, M.C., Ripoll, A., Pérez, N., Prévôt, A.S.H., Canonaco, F., Querol, X., Alastuey, A., 2015. Chemical characterization of submicron regional background aerosols in the western Mediterranean using an Aerosol Chemical Speciation Monitor. Atmos. Chem. Phys. 15, 6379–6391. https://doi.org/10.5194/acp-15-6379-2015.

Mohr, C., DeCarlo, P.F., Heringa, M.F., Chirico, R., Slowik, J.G., Richter, R., Reche, C., Alastuey, A., Querol, X., Seco, R., Peñuelas, J., Jiménez, J.L., Crippa, M., Zimmermann, R., Baltensperger, U., Prévôt, A.S.H., 2012. Identification and quantification of organic aerosol from cooking and other sources in Barcelona using aerosol mass spectrometer data. Atmos. Chem. Phys. 12, 1649–1665. https://doi.org/10.5194/acp-12-1649-2012.

Ng, N.L., Canagaratna, M.R., Jimenez, J.L., Zhang, Q., Ulbrich, I.M., Worsnop, D.R., 2011a. Real-time methods for estimating organic component mass concentrations from aerosol mass spectrometer data. Environ. Sci. Technol. 45, 910–916. https://doi.org/10.1021/es102951k.

Ng, N.L., Canagaratna, M.R., Zhang, Q., Jimenez, J.L., Tian, J., Ulbrich, I.M., Kroll, J.H., Docherty, K.S., Chhabra, P.S., Bahreini, R., Murphy, S.M., Seinfeld, J.H., Hildebrandt, L., Donahue, N.M., DeCarlo, P.F., Lanz, V.A., Prévôt, A.S.H., Dinar, E., Rudich, Y., Worsnop, D.R., 2010. Organic aerosol components observed in Northern Hemispheric datasets from Aerosol Mass Spectrometry. Atmos. Chem. Phys. 10, 4625–4641. https://doi.org/10.5194/acp-10-4625-2010.

Ng, N.L., Herndon, S.C., Trimborn, A., Canagaratna, M.R., Croteau, P.L., Onasch, T.B., Sueper, D., Worsnop, D.R., Zhang, Q., Sun, Y.L., Jayne, J.T., 2011b. An Aerosol Chemical Speciation Monitor (ACSM) for routine monitoring of the composition and mass concentrations of ambient aerosol. Aerosol Sci. Technol. 45, 780–794. https://doi.org/10.1080/02786826.2011.560211.

Paatero, P., 1999. The multilinear engine—a table-driven, least squares program for solving multilinear problems, including the n -way parallel factor analysis model. J. Comput. Graph. Stat. 8, 854–888. https://doi.org/10.1080/10618600.1999.10474853.

Paatero, P., Eberly, S., Brown, S.G., Norris, G.A., 2014. Methods for estimating uncertainty in factor analytic solutions. Atmos. Meas. Tech. 7, 781–797. https://doi.org/10.5194/amt-7-781-2014.

Paatero, P., Hopke, P.K., 2009. Rotational tools for factor analytic models. J. Chemom. 23, 91–100. https://doi.org/10.1002/cem.1197.

Paatero, P., Hopke, P.K., Song, X.-H., Ramadan, Z., 2002. Understanding and controlling rotations in factor analytic models. Chemom. Intell. Lab. Syst. 60, 253–264. https://doi.org/10.1016/S0169-7439(01)00200-3.

Paatero, P., Tapper, U., 1994. Positive matrix factorization: a non-negative factor model with optimal utilization of error estimates of data values. Environmetrics 5, 111–126. https://doi.org/10.1002/env.3170050203.

Parworth, C., Fast, J., Mei, F., Shippert, T., Sivaraman, C., Tilp, A., Watson, T., Zhang, Q., 2015. Long-term measurements of submicrometer aerosol chemistry at the Southern Great Plains (SGP) using an Aerosol Chemical Speciation Monitor (ACSM). Atmos. Environ. 106, 43–55. https://doi.org/10.1016/j.atmosenv.2015.01.060.

Petit, J.-E., Dupont, J.-C., Favez, O., Gros, V., Zhang, Y., Sciare, J., Simon, L., Truong, F., Bonnaire, N., Amodeo, T., Vautard, R., Haeffelin, M., 2021. Response of atmospheric composition to COVID-19 lockdown measures during spring in the Paris region (France). Atmos. Chem. Phys. 21, 17167–17183. https://doi.org/10.5194/acp-21-17167-2021.

Pfaffenberger, L., Barmet, P., Slowik, J.G., Praplan, A.P., Dommen, J., Prévôt, A.S.H., Baltensperger, U., 2013. The link between organic aerosol mass loading and degree of oxygenation: an α-pinene photooxidation study. Atmos. Chem. Phys. 13, 6493–6506. https://doi.org/10.5194/acp-13-6493-2013.

Pieber, S.M., El Haddad, I., Slowik, J.G., Canagaratna, M.R., Jayne, J.T., Platt, S.M., Bozzetti, C., Daellenbach, K.R., Fröhlich, R., Vlachou, A., Klein, F., Dommen, J., Miljevic, B., Jiménez, J.L., Worsnop, D.R., Baltensperger, U., Prévôt, A.S.H., 2016. Inorganic salt interference on CO_2^+ in Aerodyne AMS and ACSM organic aerosol composition studies. Environ. Sci. Technol. 50, 10494–10503. https://doi.org/10.1021/acs.est.6b01035.

Poulain, L., Spindler, G., Grüner, A., Tuch, T., Stieger, B., van Pinxteren, D., Petit, J.-E., Favez, O., Herrmann, H., Wiedensohler, A., van Pinxteren, D., Herrmann, H., Wiedensohler, A., 2020. Multi-year ACSM measurements at the central European research station Melpitz (Germany) – Part 1: instrument robustness, quality assurance, and impact of upper size cutoff diameter. Atmos. Meas. Tech. 13, 4973–4994. https://doi.org/10.5194/amt-13-4973-2020.

Qi, L., Chen, M., Stefenelli, G., Pospisilova, V., Tong, Y., Bertrand, A., Hueglin, C., Ge, X., Baltensperger, U., Prévôt, A.S.H., Slowik, J.G., 2019. Organic aerosol source apportionment in Zurich using an extractive electrospray ionization time-of-flight mass spectrometer (EESI-TOF-MS) - Part 2: biomass burning influences in winter. Atmos. Chem. Phys. 19, 1–42. https://doi.org/10.5194/acp-19-8037-2019.

Sandradewi, J., Prévôt, A.S.H., Szidat, S., Perron, N., Alfarra, M.R., Lanz, V.A., Weingartner, E., Baltensperger, U., 2008. Using aerosol light absorption measurements for the quantitative determination of wood burning and traffic emission contributions to particulate matter. Environ. Sci. Technol. 42, 3316–3323. https://doi.org/10.1021/es702253m.

Stavroulas, I., Bougiatioti, A., Grivas, G., Paraskevopoulou, D., Tsagkaraki, M., Zarmpas, P., Liakakou, E., Gerasopoulos, E., Mihalopoulos, N., 2019. Sources and processes that control the submicron organic aerosol composition in an urban Mediterranean environment (Athens): a high temporal-resolution chemical composition measurement study. Atmos. Chem. Phys. 19, 901–919. https://doi.org/10.5194/acp-19-901-2019.

Stefenelli, G., Pospisilova, V., Lopez-Hilfiker, F.D., Daellenbach, K.R., Hüglin, C., Tong, Y., Baltensperger, U., Prevot, A.S.H., Slowik, J.G., 2019. Organic aerosol source apportionment in Zurich using an extractive electrospray ionization time-of-flight mass spectrometer (EESI-TOF-MS) - Part 1: biogenic influences and day-night chemistry in summer. Atmos. Chem. Phys. 19, 14825–14848. https://doi.org/10.5194/acp-19-14825-2019.

Stull, R.B., 1988. An Introduction to Boundary Layer Meteorology, 1st ed. Springer, Dordrecht Netherlands, Dordrecht. 10.1007/978-94-009-3027-8.

Sun, Y., Du, W., Fu, P., Wang, Q., Li, J., Ge, X., Zhang, Q., Zhu, C., Ren, L., Xu, W., Zhao, J., Han, T., Worsnop, D.R., Wang, Z., 2016. Primary and secondary aerosols in Beijing in winter: sources, variations and processes. Atmos. Chem. Phys. 16, 8309–8329. https://doi.org/10.5194/acp-16-8309-2016.

Tiitta, P., Leskinen, A., Hao, L., Yli-Pirilä, P., Kortelainen, M., Grigonyte, J., Tissari, J., Lamberg, H., Hartikainen, A., Kuuspalo, K., Kortelainen, A.-M., Virtanen, A., Lehtinen, K.E.J., Komppula, M., Pieber, S., Prévôt, A.S.H., Onasch, T.B., Worsnop, D.

R., Czech, H., Zimmermann, R., Jokiniemi, J., Sippula, O., 2016. Transformation of logwood combustion emissions in a smog chamber: formation of secondary organic aerosol and changes in the primary organic aerosol upon daytime and nighttime aging. Atmos. Chem. Phys. 16, 13251–13269. https://doi.org/10.5194/acp-16-13251-2016.

Tobler, A.K., Skiba, A., Canonaco, F., Močnik, G., Rai, P., Chen, G., Bartyzel, J., Zimnoch, M., Styszko, K., Nęcki, J., Furger, M., Różański, K., Baltensperger, U., Slowik, J.G., Prevot, A.S.H., 2021. Characterization of non-refractory (NR) PM$_1$ and source apportionment of organic aerosol in Kraków. Atmos. Chem. Phys. 21, 14893–14906. https://doi.org/10.5194/acp-21-14893-2021.

Ulbrich, I.M., Canagaratna, M.R., Zhang, Q., Worsnop, D.R., Jimenez, J.L., 2009. Interpretation of organic components from Positive Matrix Factorization of aerosol mass spectrometric data. Atmos. Chem. Phys. 9, 2891–2918. https://doi.org/10.5194/acp-9-2891-2009.

Via, M., Minguillón, M.C., Reche, C., Querol, X., Alastuey, A., 2021. Increase in secondary organic aerosol in an urban environment. Atmos. Chem. Phys. 21, 8323–8339. https://doi.org/10.5194/acp-21-8323-2021.

Weimer, S., Alfarra, M.R., Schreiber, D., Mohr, M., Prévôt, A.S.H., Baltensperger, U., 2008. Organic aerosol mass spectral signatures from wood-burning emissions: Influence of burning conditions and wood type. J. Geophys. Res. 113, D10304. https://doi.org/10.1029/2007JD009309.

World Health Organization, 2021. WHO global air quality guidelines. Particulate matter (PM$_{2.5}$ and PM$_{10}$), ozone, nitrogen dioxide, sulfur dioxide and carbon monoxide. Geneva.

Xie, M., Hannigan, M.P., Barsanti, K.C., 2014. Gas/Particle Partitioning of 2-Methyltetrols and Levoglucosan at an Urban Site in Denver. Environ. Sci. Technol. 48, 2835–2842. https://doi.org/10.1021/es405356n.

Xu, W., Croteau, P., Williams, L., Canagaratna, M., Onasch, T., Cross, E., Zhang, X., Robinson, W., Worsnop, D., Jayne, J., 2017. Laboratory characterization of an aerosol chemical speciation monitor with PM 2.5 measurement capability. Aerosol Sci. Technol. 51, 69–83. https://doi.org/10.1080/02786826.2016.1241859.

Yang, Y., Wang, H., Smith, S.J., Zhang, R., Lou, S., Yu, H., Li, C., Rasch, P.J., 2018. Source apportionments of aerosols and their direct radiative forcing and long-term trends over continental United States. Earth's Futur. 6, 793–808. https://doi.org/10.1029/2018EF000859.

Yang, Y., Ruan, Z., Wang, X., Yang, Y., Mason, T.G., Lin, H., Tian, L., 2019. Short-term and long-term exposures to fine particulate matter constituents and health: a systematic review and meta-analysis. Environ. Pollut. 247, 874–882. https://doi.org/10.1016/j.envpol.2018.12.060.

Yli-Juuti, T., Mielonen, T., Heikkinen, L., Arola, A., Ehn, M., Isokääntä, S., Keskinen, H.-M., Kulmala, M., Laakso, A., Lipponen, A., Luoma, K., Mikkonen, S., Nieminen, T., Paasonen, P., Petäjä, T., Romakkaniemi, S., Tonttila, J., Kokkola, H., Virtanen, A., 2021. Significance of the organic aerosol driven climate feedback in the boreal area. Nat. Commun. 12, 5637. https://doi.org/10.1038/s41467-021-25850-7.

Yttri, K.E., Canonaco, F., Eckhardt, S., Evangeliou, N., Fiebig, M., Gundersen, H., Hjellbrekke, A.-G., Lund Myhre, C., Platt, S.M., Prévôt, A.S.H., Simpson, D., Solberg, S., Surratt, J., Tørseth, K., Uggerud, H., Vadset, M., Wan, X., Aas, W., 2021. Trends, composition, and sources of carbonaceous aerosol at the Birkenes Observatory, northern Europe, 2001–2018. Atmos. Chem. Phys. 21, 7149–7170. https://doi.org/10.5194/acp-21-7149-2021.

Zhang, Q., Jimenez, J.L., Canagaratna, M.R., Allan, J.D., Coe, H., Ulbrich, I., Alfarra, M. R., Takami, A., Middlebrook, A.M., Sun, Y.L., Dzepina, K., Dunlea, E., Docherty, K., DeCarlo, P.F., Salcedo, D., Onasch, T., Jayne, J.T., Miyoshi, T., Shimono, A., Hatakeyama, S., Takegawa, N., Kondo, Y., Schneider, J., Drewnick, F., Borrmann, S., Weimer, S., Demerjian, K., Williams, P., Bower, K., Bahreini, R., Cottrell, L., Griffin, R.J., Rautiainen, J., Sun, J.Y., Zhang, Y.M., Worsnop, D.R., 2007. Ubiquity and dominance of oxygenated species in organic aerosols in anthropogenically-influenced Northern Hemisphere midlatitudes. Geophys. Res. Lett. 34 (13) https://doi.org/10.1029/2007GL029979.

Zhang, Q., Jimenez, J.L., Canagaratna, M.R., Ulbrich, I.M., Ng, N.L., Worsnop, D.R., Sun, Y., 2011. Understanding atmospheric organic aerosols via factor analysis of aerosol mass spectrometry: a review. Anal. Bioanal. Chem. 401, 3045–3067. https://doi.org/10.1007/s00216-011-5355-y.

Zhang, Y., Albinet, A., Petit, J.-E., Jacob, V., Chevrier, F., Gille, G., Pontet, S., Chrétien, E., Dominik-Sègue, M., Levigoureux, G., Močnik, G., Gros, V., Jaffrezo, J.-L., Favez, O., 2020. Substantial brown carbon emissions from wintertime residential wood burning over France. Sci. Total Environ. 743, 140752 https://doi.org/10.1016/j.scitotenv.2020.140752.

Zhang, Y., Favez, O., Petit, J.-E., Canonaco, F., Truong, F., Bonnaire, N., Crenn, V., Amodeo, T., Prévôt, A.S.H., Sciare, J., Gros, V., Albinet, A., 2019. Six-year source apportionment of submicron organic aerosols from near-continuous highly time-resolved measurements at SIRTA (Paris area, France). Atmos. Chem. Phys. 19, 14755–14776. https://doi.org/10.5194/acp-19-14755-2019.

Zotter, P., Herich, H., Gysel, M., El-Haddad, I., Zhang, Y., Močnik, G., Hüglin, C., Baltensperger, U., Szidat, S., Prévôt, A.S.H., 2017. Evaluation of the absorption Ångström exponents for traffic and wood burning in the Aethalometer-based source apportionment using radiocarbon measurements of ambient aerosol. Atmos. Chem. Phys. 17, 4229–4249. https://doi.org/10.5194/acp-17-4229-2017.